J. Fac. Pharm. Ankara / Ankara Ecz. Fak. Derg., 48(2): 412-435, 2024
Doi: 10.33483/jfpau.1354293

ORIGINAL ARTICLE / ÖZGÜN MAKALE

PHYTOCHEMICAL PROFILING, ANTIOXIDANT, ANTIDIABETIC, AND ADMET STUDY OF *DIOSPYROS MESPILIFORMIS* HOCHST. EX A. DC. (EBENACEAE) LEAF

DIOSPYROS MESPILIFORMIS HOCHST. EX A. DC. (EBENACEAE) YAPRAKLARININ FİTOKİMYASAL PROFİLLENDİRMESİ, ANTİOKSİDAN, ANTİDİYABETİK VE ADMET ÇALIŞMASI

Mubarak Muhammad DAHIRU[1]*, Neksumi MUSA[2]

[1]Adamawa State Polytechnic, School Science and Technology, Department of Pharmaceutical Technology, 640101, Yola, Nigeria
[2]Adamawa State Polytechnic, School Science and Technology, Department of Science Laboratory Technology, 640101, Yola, Nigeria

ABSTRACT

Objective: *This study aimed to carry out phytochemical profiling, antioxidant, antidiabetic, and ADMET study on the crude ethanol extract (CR) of Diospyros mespiliformis (DM) and its ethyl acetate (EEF) and aqueous fractions (AQF).*
Material and Method: *The phytochemicals were identified by GC-MS. The antioxidant activity was determined in vitro and silico while the antidiabetic and ADMET were in silico.*
Result and Discussion: *Exactly 54 and 44 compounds were respectively identified in the EEF and AQF. At 300 µg/ml, the CR demonstrated a significantly ($p < 0.05$) higher ascorbic acid equivalent (AAE) total antioxidant capacity (TAC) (73.59 ± 0.011 µg/ml) than the EEF (41.28 ± 0.003 µg/ml AAE) and AQF (31.28 ± 0.005 µg/ml AAE). The total reducing power (TRP) of the AQF (106.84 ± 3.46 µg/ml) was significantly ($p <0.05$) higher than the CR (93.23 ± 5.63 µg/ml AAE) and EEF (92.35 ± 6.96 µg/ml AAE) at 100 µg/ml. A significantly ($p < 0.05$) higher percentage inhibition (48.38% ± 4.61) was demonstrated by the EEF at 1 mg/ml in the ferric thiocyanate and a lower malonaldehyde concentration (0.75 ± 0.01 nmol/ml) in the thiobarbituric acid methods. The AQF demonstrated a significantly ($p < 0.05$) higher (82.72% ± 1.88) peroxide scavenging activity at 100 µg/ml than the CR (33.33% ± 2.16) and EEF (63.64% ± 2.66). Compound VII exhibited the lowest binding affinity (BA) and inhibition constant (Ki) of -8.8 kcal/mol and 0.35 µM, respectively with xanthine oxidase and -8.0 kcal/mol and 1.35 µM, respectively with NADH oxidase. X exhibited the lowest BA (-8.5 kcal/mol) and Ki (0.58 µM) interacting with CytP450 21A2. Compound III exhibited the lowest BA (-7.5 kcal/mol) and Ki (3.14 µM) with PTP1B while compound X had BA and Ki values of -8.5 kcal/mol and 0.58 µM, respectively with PPARγ. The result of ADMET showed some of the compounds might be strong candidates for antioxidant and antidiabetic drugs. All the extracts possess significant antioxidant activity and some of the identified compounds might be candidates for novel antioxidants and antidiabetic drugs.*
Keywords: *ADMET, antidiabetic, antioxidant, molecular docking, molecular dynamics*

* **Corresponding Author / Sorumlu Yazar:** Mubarak Muhammad Dahiru
e-mail / e-posta: mubaraq93@adamawapoly.edu.ng, **Phone / Tel.:** +2348036508768

Submitted / Gönderilme : 02.09.2023
Accepted / Kabul : 22.01.2024
Published / Yayınlanma : 20.05.2024

ÖZ

Amaç: *Bu çalışmada Diospyros mespiliformis (DM) ham etanol ekstraktı (CR), etil asetat (EEF) ve sulu fraksiyonları (AQF) üzerinde fitokimyasal profilleme, antioksidan, antidiyabetik ve ADMET çalışmasının yapılması amaçlandı.*

Gereç ve Yöntem: *Fitokimyasallar GC-MS ile tanımlandı. Antioksidan aktivite in vitro ve silico olarak belirlenirken, antidiyabetik ve ADMET in silico olarak belirlendi.*

Sonuç ve Tartışma: *EEF ve AQF'de sırasıyla tam olarak 54 ve 44 bileşik tanımlandı. 300 µg/ml'de CR (73.59 ± 0.011 µg/ml), EEF (41.28 ± 0.003 µg/ml AAE) ve AQF (31.28 ± 0.005 µg/ml AAE)'den önemli ölçüde ($p<0.05$) daha yüksek askorbik asit eşdeğeri (AAE) toplam antioksidan kapasitesi (TAC) gösterdi. 100 µg/ml'de AQF'nin (106.84 ± 3.46 µg/ml) toplam indirgeme gücü (TRP), CR'den (93.23 ± 5.63 µg/ml AAE) ve EEF'den (92.35 ± 6.96 µg/ml AAE) önemli ölçüde ($p <0.05$) daha yüksekti. 1 mg/ml EEF, ferrik tiyosiyanat yönteminde önemli ölçüde ($p<0.05$) daha yüksek bir inhibisyon yüzdesi (%48.38 ±4.61) ve tiyobarbitürik asit yönteminde daha düşük bir malonaldehid konsantrasyonu (0.75 nmol/ml ±0.01) gösterdi. AQF, 100 µg/ml'de CR (%33.33 ± 2.16) ve EEF'den (%63.64 ± 2.66) önemli ölçüde ($p < 0.05$) daha yüksek (%82.72 ± 1.88) peroksit temizleme aktivitesi gösterdi. Bileşik VII, ksantin oksidaz ile sırasıyla -8.8 kcal/mol ve 0.35 µM ve NADH oksidaz ile sırasıyla -8.0 kcal/mol ve 1.35 µM ile en düşük bağlanma afinitesini (BA) ve inhibisyon sabitini (Ki) sergiledi. X, CytP450 21A2 ile etkileşime giren en düşük BA (-8.5 kcal/mol) ve Ki'yi (0.58 uM) sergiledi. Bileşik III, PTP1B ile en düşük BA (-7.5 kcal/mol) ve Ki'yi (3.14 µM) sergilerken; bileşik X, PPARy ile sırasıyla -8.5 kcal/mol ve 0.58 µM BA ve Ki değerlerine sahipti. ADMET sonucu, bazı bileşiklerin antioksidan ve antidiyabetik ilaçlar için güçlü adaylar olabileceğini gösterdi. Tüm ekstraktlar önemli antioksidan aktiviteye sahiptir ve tanımlanan bileşiklerin bazıları yeni antioksidanlar ve antidiyabetik ilaçlar için aday olabilir.*

Anahtar Kelimeler: *ADMET, antidiyabetik, antioksidan, moleküler yerleştirme, moleküler dinamik*

INTRODUCTION

Diabetes entails endocrine metabolic disorders characterized by a loss of glycemic control leading to the development of acute and subsequent chronic complications, including macro- and micro-vascular complications [1,2]. Various strategies are employed in the management of diabetes including synthetic drugs to achieve glycemic control. However, proper diet and exercise are the usual recommendations. Synthetic drugs employed in the management of diabetes are often reported to possess side effects, thus undesirable for prolonged use [3]. Furthermore, the specificity of these drugs towards their target and the nature of diabetes as a metabolic disorder makes a single therapy a challenge for some individuals. The need for combined therapy leads to more side effects [3]. Additionally, the cost of diabetic therapy is often expensive for some individuals, especially in low-income countries [4,5]. Therefore, the need for an affordable, safe, and efficient alternative.

Drugs from plant sources are often considered as alternate sources especially for low-income countries and rural communities due to their efficacy and low cost with minimized side effects. The use of plant-based drugs in diabetes is due to their phytoconstituents associated with various individual and synergistic modes of action [6]. In some cases, these phytoconstituents are isolated and studied for their antidiabetic activities while in others as crude extracts [6]. Identification of these compounds has gained attention in recent times as these compounds are sources of novel drugs for the management of ailments [7]. Different studies previously reported the application of different plants and compounds of plant origin with antidiabetic activities. These studies often involve animal models and in other cases *in vitro* studies to justify their use in folkloric medicine [8-13]. Furthermore, in traditional practice, plants of different types including *D. mespiliformis* are formulated in various preparations, including decoction and maceration to extract these compounds for medicinal applications.

D. mespiliformis is a plant native to West Africa and often called West African ebony or African ebony. It is an evergreen tree growing up to 25 meters in drylands, often used as a source of food because of its edible fruit and for medicinal purposes [14]. In folkloric medicine, the roots and bark of the plant are employed in the treatment of infections, toothaches, fever, wound healing, malaria, leprosy, and headache [15]. Furthermore, previous studies reported that the plant exerts pharmacological activities, including hypoglycemic, antioxidant, neuropharmacological, analgesic, antiproliferative, and

antimicrobial properties [16]. However, the determination of the activity and identification of the constituent compounds of the different fractions of the plant present gaps in knowledge. This includes the interactions of these constituents with the proteins involved in the pathology of oxidative stress and diabetes. Additionally, the ADMET properties of the compounds also present unexplored gaps. Thus, in our study, we investigated the phytochemical profile, antioxidant, antidiabetic, and ADMET properties of the crude ethanol extract (CR) of *Diospyros mespiliformis* and its ethyl acetate (EEF) and aqueous fractions (AQF). Additionally, we investigated the ADMET properties of the identified compounds and their interaction with different antioxidant and antidiabetic targets.

MATERIAL AND METHOD

Sample Collection and Preparation

Fresh leaves sample of *D. mespiliformis* (DM) was obtained from Mayo-belwa local government of Adamawa State. The plant was authenticated by a Forest technologist with a voucher specimen (ASP/FT/078) deposited in the Department of Forestry Technology. The plant was air-dried and ground to powder then 7 days of maceration of 1 kg of the powder in 70% (v/v) ethanol. This was followed by filtering and concentrating the filtrate to dryness at 40ºC with a rotary evaporator (Buchi Rotavapor R-200) yielding 150 g of the crude extract (green-colored).

Extract Fractionation

Exactly 100 g of the crude extract (CR) was completely dissolved in 250 ml of distilled water and transferred to a separating funnel for partitioning with ethyl acetate until a clear ethyl acetate layer was observed. The ethyl acetate layer was collected as the ethyl acetate fraction (EEF) while the aqueous layer as the aqueous fraction (AQF). Both fractions were subjected to the same drying procedure stated for the CR yielding 28.04 g of EEF (reddish brown color) and 67.12 g of AQF (dark green color). The extract and its fractions were stored at 4°C until needed for analysis.

Phytochemical Screening

The secondary metabolites (phytochemicals), including alkaloids, saponins, steroids, glycosides, terpenoids, and flavonoids were detected by the methods previously described by Evans [17] to ascertain their presence or absence.

Gas Chromatography-Mass Spectroscopy (GC-MS) Analysis

A combined GC-MS (Agilent 19091-433HP, USA) fused with a silica column was used to identify the compounds present in DM. The procedures and instrumentation settings were as we described previously [18].

Antioxidant Assay

Total Antioxidant Capacity (TAC)

The TAC of the samples was determined according to the protocol described by Prieto *et al.*, [19]. Briefly, 0.5 ml of the sample (300 µg/ml) was incubated with the phosphor-molybdate reagent while the same volume of varying concentrations (20-100 µg/ml) of ascorbic acid [AA (standard)] was used to obtain the standard calibration curve of concentration versus absorbance. The blank was made up of the phosphor-molybdate reagent and distilled water incubated in the same condition as the sample and AA. The TAC of the samples was expressed as AA equivalent (AAE) in µg/ml. All values were determined in triplicates.

Total Reducing Power (TRP)

The protocol described by Oyaizu [20] was employed to determine the TRP of samples. Briefly, 0.25 ml of the sample (100 µg/ml) dissolved in distilled water was used while the same volume of varying concentrations of AA (20-100 µg/ml) incubated similarly to the samples was used to obtain the AA calibration curve. The blank was a mixture of the reagents without samples. The TRP was expressed

as AAE in µg/ml. All values were determined in triplicates.

Ferric Thiocyanate Method (FTC)

The procedure described previously by Kikuzaki and Nakatani [21] was employed to determine the lipid peroxidation inhibitory potential of the samples. Briefly, 4 ml of the sample (1 mg/ml) dissolved in absolute ethanol was used whereas the same volume and concentration of AA dissolved in absolute ethanol was used as a standard. A mixture without the sample was used as blank. The percentage inhibition was determined according to Equation 1 [22]. All values were determined in triplicates.

$$\% \text{ Inhibition} = 100 - \frac{\text{At}}{\text{Ac}}\ x\ 100 \qquad \text{Equation 1}$$

Where At = Absorbance of sample while Ac = Absorbance of control

Thiobarbituric Acid Method (TBA)

The protocol described by Kikuzaki and Nakatani [21] was adopted to further determine the anti-lipid peroxidation effects of the samples. Briefly, 1 ml of 1 mg/ml of the sample and ascorbic acid (AA) solutions from the FTC method were used with AA regarded as a standard while the mixture without sample was blank. The malonaldehyde (MDA) concentration was determined by equation 2 using the extinction coefficient 156 mM^{-1} cm^{-1} as previously described [23]. All values were determined in triplicates.

$$\text{MDA concentration} = \frac{\text{OD}}{\text{EC}}\ x\ \text{Sample volume} \qquad \text{Equation 2}$$

Where OD = Absorbance of the sample while EC = Extinction coefficient

Hydrogen Peroxide (H_2O_2) Scavenging Assay

The procedure described by Zang [24] was followed to determine the H_2O_2 scavenging potential of the samples. Briefly, 2 ml of varying concentrations (20-100 µg/ml) of the sample and AA was used with AA regarded as a standard while the reaction mixture without the sample was used as a blank for the titration. All values were determined in triplicates.

***In silico* Study**

Drug-likeness

The identified compounds were further screened for drug-like properties and subjected to molecular docking and molecular dynamics studies. The drug-likeness screening was carried out using the DruLiTo software by applying Lipinski's rule, Veber rule, and Ghose Filter. Only compounds that passed Lipinski's rule and either Veber or Ghose filters were further subjected to the molecular docking and molecular dynamics study.

Molecular Docking (MD) and Molecular Dynamics Simulation (MDS)

The compounds were downloaded from the PubChem website in SDF formats and energy-minimized by PyRx software (PyRx- Python Prescription 0.8) for molecular docking. The docking pockets were identified using the PrankWeb: Ligand Binding Site Prediction online server [24]. The target proteins were downloaded from the RSCB protein data bank website and prepared using the AutoDockTools software version 1.5.7 [25] by removing identical chains, heteroatoms, and water molecules. The PyRx software was used for the molecular docking where only the top 10 compounds with the lowest binding energy (BA) were selected. The 2D and 3D interactions of the docked complexes were depicted using the LigPlot$^+$ (version 2.2.8.) [27] and PyMol (Version 2.0 Schrödinger, LLC) softwares, respectively while the salt bridges were identified using the Protein-Ligand Interaction Profiler online server [28]. The compounds with their PubChem ID are listed in Table 1 while the targets, including their PDB IDs and docking coordinates in Table 2. The molecular dynamics simulations were done with the Webnm online server [29] to determine the chain and residue displacements of the docked complexes with the lowest BA identified above. The inhibition constant was determined from the BA

by the equation; Ki=exp ΔG/RT, where T=298.15 K (temperature), R=1.985 x 10^{-3} $kcal^{-1}$ mol^{-1} k^{-1} (the universal gas constant), and ΔG=binding affinity [30].

Table 1. List of the compounds screened for drug-likeness

Names of the Compounds	Designation	PubChem ID
(2,2,6-trimethylbicyclo [4.1.0] hept-1-yl) methanol	I	535115
1-(4-Bromobutyl)-2-piperidinone	II	536377
4a-methyl-7-(propan-2-yl) octahydronaphthalen-2(1H)-one	III	41133
2,3-Dimethylfluorobenzene	IV	96489
2,7-Octanedione	V	74196
3-(Acetyloxy)-2-isopropyl-2-methyl butyl acetate	VI	538234
3-(azepan-1-yl)-1,2-benzothiazole 1,1-dioxide	VII	535203
4-Phenylpiperidine	VIII	69873
Butyraldehyde, semicarbazone	IX	9601714
Caryophyllene oxide	X	1742210
cis-(Z)-alpha.-Bisabolene epoxide	XI	91753574
Cubedol	XII	11276107
Ethyl 4-isopropenyl-6-methyl-2-oxo-6-heptenoate	XIII	543224
Farnesol	XIV	445070
Isometheptene	XV	22297
Lilac alcohol A	XVI	526973

Table 2. List of docking targets for the MD

Activity	Target	PDB ID	Docking coordinates		
			X	Y	Z
Antioxidant	Xanthine Oxidase (XO)	3NVZ	23.23	-16.02	35.78
	Cytochrome P450 21A2 (CytP450 21A2)	4Y8W	-14.71	12.04	28.68
	NADH Oxidase (NOX)	5ER0	-6.76	-53.62	50.91
Antidiabetic	Protein tyrosine phosphatase 1B (PTP1B)	2ZMM	46.08	15.49	3.12
	Peroxisome proliferator-activated receptor gamma (PPARγ)	4EMA	14.16	6.91	44.56

ADMET Study

The compounds with top interactions (lowest BA) identified from the MD were further screened for drug-like properties, including absorption, distribution, metabolism, excretion, and toxicity (ADMET) using the pkCSM – pharmacokinetics online server [31].

Statistics

The results obtained were expressed as mean ± standard error of the mean (± SEM) and statistically evaluated by one-way analysis of variance followed by Tukey's multiple comparison tests at $p < 0.05$ level of significance. The statistical analysis was carried out using the Statistical Package for Social Sciences (SPSS) version 22 software.

RESULT AND DISCUSSION

The phytochemical components of the CR, EEF, and AQF of the DM leaf are shown in Table 3. Alkaloids and steroids were detected in the CR and EEF only. Saponins were detected in the CR and its fractions while flavonoids were absent in the EEF.

Phytochemicals have different affinity for different solvents depending on the solvent polarity and the type of phytochemical extracted depends on the solvent employed during extraction [33-34]. Moreover, during the partitioning process, the phytochemicals with higher affinity towards a solvent will partition in that solvent [35-37]. Thus, saponins detected in all the solvents might be attributed to

their amphiphilic nature and affinity towards ethyl acetate and water. The detection of flavonoids in only the CR and AQF might be due to the presence of polar flavonoids. Moreover, the steroids detected might be hydrophobic, thus, they were not detected in the AQF. Similar results were previously reported [38,39].

Table 3. Phytochemical composition of CR, EEF, and AQF of DM leaf

Phytochemical	CR	EEF	AQF
Alkaloids	+	+	-
Saponins	+	+	+
Steroids	+	+	-
Glycosides	-	-	-
Terpenoids	-	-	-
Flavonoids	+	-	+

*(+: Present, -: Absent)

GC-MS Analysis

Table 4 shows the identified compounds in the EEF of DM. Exactly 54 compounds were identified in the EEF of DM made up of mostly long-chain aliphatic and aromatic compounds. Squalene was the most abundant (33.41%) next to Lilac alcohol A and Caryophyllene oxide with peak areas of 13.23 and 5.17 %, respectively. The least abundant compound was 8-Methylenepentadecane (0.01%). Furthermore, Figure 1 shows the structures of the compounds while the GC-MC chromatogram is shown in 3a.

Squalene identified as the most abundant compound in the EEF of DM might be attributed it its non-polar nature as ethyl acetate is a moderately polar solvent. Thus, extracting squalene in higher abundance than distilled water (AQF) [32-34]. Moreover, this compound has been associated with pharmacological actions against hypoglycemia, LDL-C, and cardiovascular diseases [40]. Therefore, it might contribute to the antidiabetic effects reported in our study. Lilac alcohol A (2-(5-Methyl-5-vinyltetrahydro-2-furanyl)-1-propanol) is another compound detected in the EEF next to squalene in abundance which might be due to its moderate solubility. Caryophyllene oxide is another moderately soluble compound identified in the EEF in high abundance. This compound has been previously reported to exert antidiabetic [41], antioxidant activities [41], and anti-obesity [42] activities. Therefore, it might also be a notable contributor to the antidiabetic effect reported in our study. Moreover, some of the compounds reported were previously associated with antidiabetic properties including, humulene [43], Caryophyllene [44], Nerolidol [45], Farnesol [46], and 2- Chloropropionic acid, octadecyl ester [47].

Table 5 presents the compounds identified in the AQF of DM. Exactly 44 compounds were identified with linoleic acid as the most abundant with a peak area of 29.86% next to palmitic acid (15.13%) and phytol (5.90%) while 2, 7-Octanedione was the least abundant (0.02%). Additionally, the structure of the identified compounds in the AQF is presented in Figure 2 while Figure 3b shows the GC-MS chromatogram.

Linoleic acid, palmitic acid, and phytol were detected in high abundance in the AQF. These compounds were not partitioned into the EEF and, thus, left in the AQF. Linoleic acid (an omega-6 fatty acid) has been previously reported to exert hypoglycemic effects in diabetic rats [48]. Additionally, some of the identified compounds in AQF were reported to exert antidiabetic effects including squalene [49].

Table 4. Compounds identified in the EEF of DM

S/N	Name	RT	Area (%)	MW
1	*N*-Nitrosopiperazine	5.12	0.02	115.13
2	8-Methylenepentadecane	5.19	0.01	224.42
3	5-Methyl-1-undecene	5.27	0.01	168.32

Table 4 (*continue*). Compounds identified in the EEF of DM

S/N	Name	RT	Area (%)	MW
4	1-Chloro-2-methylazetidine	6.82	0.03	105.56
5	4-Phenylpiperidine	6.94	0.08	161.24
6	Caryophyllene	7.26	0.83	204.35
7	Humulene	7.61	0.47	204.35
8	Santolina triene	7.72	0.08	136.23
9	2,3-Dimethylfluorobenzene	8.01	1.37	124.16
10	Cubedol	8.16	1.17	222.37
11	Nerolidol	8.48	0.46	222.37
12	Patchulane	8.67	4.29	206.37
13	4-Methylenecyclohexanemethanol	8.87	1.52	126.20
14	*(E, Z)*-alpha-Farnesene	9.12	1.70	204.35
15	Farnesol	9.27	1.10	222.37
16	Lilac alcohol A	9.61	13.23	170.25
17	Caryophyllene oxide	9.78	5.17	220.35
18	Cycloheptanone, 2-(2-methylpropylidene)-	10.09	1.13	166.26
19	Ethyl 4-isopropenyl-6-methyl-2-oxo-6-heptenoate	10.34	0.63	224.30
20	Nerolidyl propionate	10.43	0.70	278.40
21	Palmitic acid, methyl ester	10.61	1.36	270.45
22	*cis-(Z)*-alpha.-Bisabolene epoxide	10.87	0.52	220.35
23	Octadecoxy ethanol	10.95	0.68	314.55
24	Cembrane	11.15	0.20	280.53
25	1-Octacosanol	11.22	0.23	410.76
26	cis-10-Nonadecenoic acid	11.49	2.63	296.49
27	2- Chloropropionic acid, octadecyl ester	11.58	2.52	361.00
28	11-Cyclopentylheneicosane	11.73	0.95	364.69
29	Hexadecyl 2-chloropropanoate	11.93	2.51	332.95
30	17-Pentatriacontene	12.06	2.30	490.93
31	Stearyl vinyl ether	12.09	0.79	296.53
32	Eicosyl perfluorobutyrate	12.14	1.72	494.60
33	1-Bromo-11-iodoundecane	12.24	1.75	361.10
34	Docosane	12.39	2.73	310.60
35	Octadecanal	12.80	1.51	268.48
36	1,19-Eicosadiene	12.91	1.45	278.52
37	Docos-1-ene	13.16	0.96	308.58
38	*(Z, Z)* -3,13-Octadecadienyl acetate	13.19	0.31	308.50
39	Hexacos-1-ene	13.23	1.92	364.69
40	3-(azepan-1-yl)-1,2-benzothiazole 1,1-dioxide	13.53	0.64	264.35
41	Propane, 1,1,3-tricyclohexyl-	13.62	1.10	290.53
42	Octadeca-1-ene	13.87	1.20	252.48
43	Hentriacontane	14.27	0.17	436.84
44	Trichlorooctadecyl silane	15.22	0.18	387.93
45	Squalene	16.62	33.41	410.72
46	Diethyl malonic acid, monochloride, 2-acethylphenyl ester	17.24	0.41	296.74
47	Hexadecyl ether	17.91	1.22	466.87
48	Tetratriacontane	18.43	0.02	478.92
49	2,2-Dimethyl-3-(3,7,16,20-tetramethyl-heneicosa-3,7,11,15,19-pentaenyl)-oxirane	18.59	0.02	412.70
50	1,26-Dibromohexacosane	19.22	0.03	524.50
51	Octatriacontyl pentafluoropropionate	19.24	0.01	697.00
52	Octacosane	19.79	0.14	394.76
53	Hexatriacontane	19.83	0.13	506.97
54	Aspidospermidin-17-ol, 1-acetyl-19,21-epoxy-15,16-dimethoxy-	19.94	0.06	414.50

RT= Retention time, MW= Molecular weight

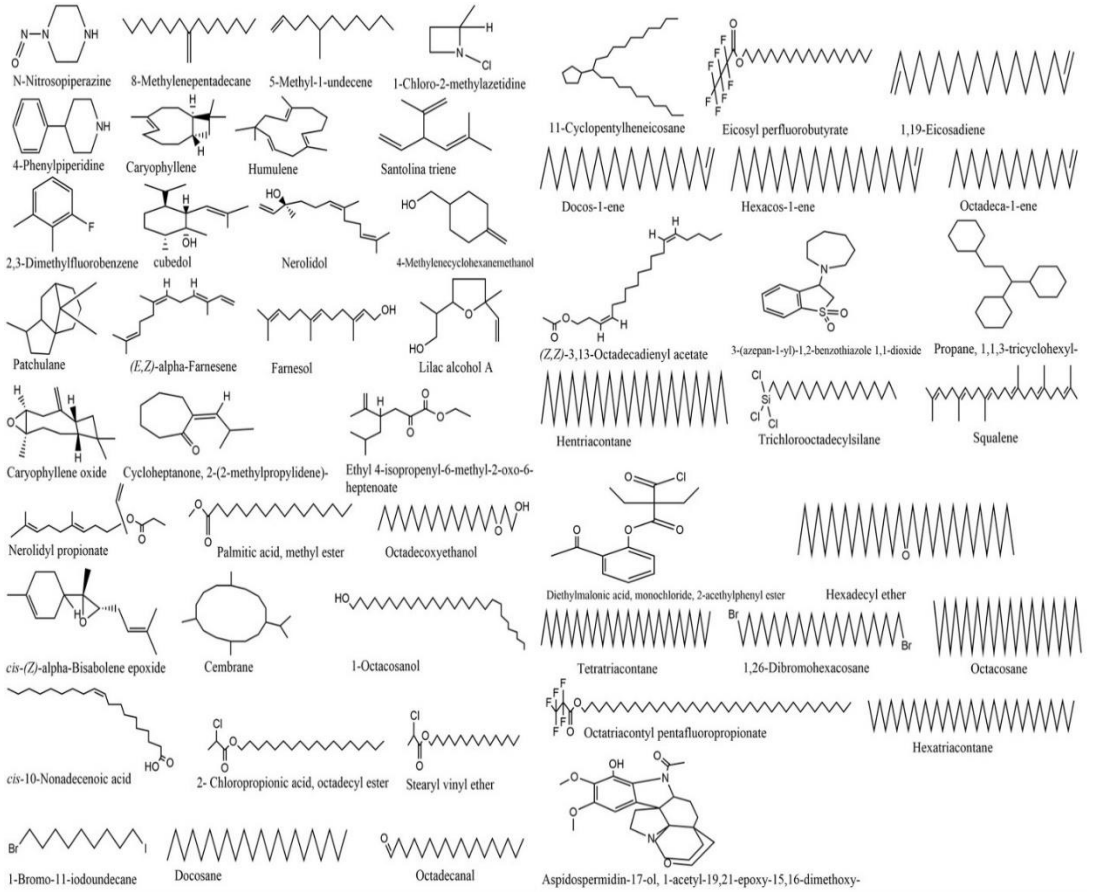

Figure 1. Structural formulas of compounds identified in the EEF of DM

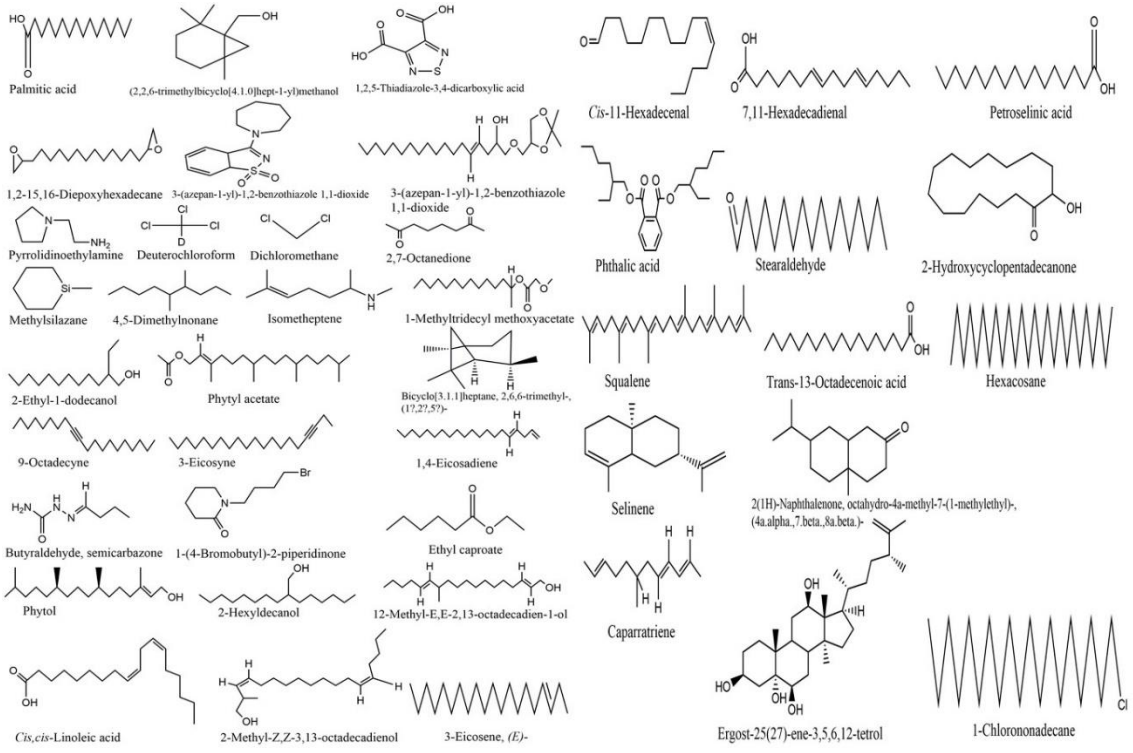

Figure 2. Structural formulars of compounds identified in the AQF of DM

Table 5. Compounds Identified in the AQF of DM

S/N	Name	RT	Area (%)	MW	Formula
1	Deuterochloroform	8.16	0.10	120.38	$CDCl_3$
2	Dichloromethane	8.79	0.13	84.93	CH_2Cl_2
3	2,7-Octanedione	9.22	0.02	142.20	$C_8H_{14}O_2$
4	Methyl silazane	11.59	0.07	113.25	$C_6H_{13}Si$
5	4,5-Dimethylnonane	13.76	0.16	156.31	$C_{11}H_{24}$
6	1,2,5-Thiadiazole-3,4-dicarboxylic acid	14.26	0.26	174.14	$C_4H_2N_2O_4S$
7	3-(Acetyloxy)-2-isopropyl-2-methylbutyl acetate	15.21	0.13	230.30	$C_{12}H_{22}O_4$
8	Isometheptene	15.44	0.07	141.25	$C_9H_{19}N$
9	1-Methyltridecyl methoxyacetate	16.46	0.55	286.40	$C_{17}H_{34}O_3$
10	Octadecan	16.58	0.74	254.49	$C_{18}H_{38}$
11	2-Ethyl-1-dodecanol	16.78	0.18	214.39	$C_{14}H_{30}O$
12	Phytyl acetate	16.89	3.13	338.6	$C_{22}H_{42}O_2$
13	Bicyclo[3.1.1]heptane, 2,6,6-trimethyl-, (1α,2β,5α)-	16.97	3.90	138.25	$C_{10}H_{18}$
14	Octadec-9-yne	17.23	0.86	250.46	$C_{18}H_{34}$
15	3-Eicosyne	17.39	1.29	278.52	$C_{20}H_{38}$
16	1,4-Eicosadiene	17.43	2.20	278.5	$C_{20}H_{38}$
17	Methyl isohexadecanoate	18.00	2.60	270.45	$C_{17}H_{34}O_2$
18	Butyraldehyde, semicarbazone	18.26	0.78	129.16	$C_5H_{11}N_3O$
19	1-(4-Bromobutyl)-2-piperidinone	18.36	1.15	234.13	$C_9H_{16}BrNO$
20	Ethyl caproate	18.64	4.95	144.21	$C_8H_{16}O_2$
21	Palmitic acid	19.11	15.13	256.42	$C_{16}H_{32}O_2$
22	Phytol	19.90	5.90	296.53	$C_{20}H_{40}O$
23	2-Hexyldecanol	20.54	1.33	242.44	$C_{16}H_{34}O$
24	*cis*,*cis*-Linoleic acid	20.90	29.86	280.45	$C_{18}H_{32}O_2$
25	12-Methyl-*E*,*E*-2,13-octadecadien-1-ol	21.88	0.12	280.50	$C_{19}H_{36}O$
26	2-Methyl-*Z*,*Z*-3,13-octadecadienol	21.95	1.48	280.5	$C_{19}H_{36}O$
27	3-Eicosene, *(E)*-	22.28	0.91	280.53	$C_{20}H_{40}$
28	*cis*-11-Hexadecenal	22.96	0.68	238.41	$C_{16}H_{30}O$
29	1,2-15,16-Diepoxyhexadecane	23.10	0.35	254.41	$C_{16}H_{30}O_2$
30	7,11-Hexadecadienal	23.41	0.46	236.39	$C_{16}H_{28}O$
31	Phthalic acid	23.54	1.72	390.56	$C_{24}H_{38}O_4$
32	Petroselinic acid	23.98	0.67	282.46	$C_{18}H_{34}O_2$
33	Stearaldehyde	25.05	0.18	268.48	$C_{18}H_{36}O$
34	2-Hydroxycyclopentadecanone	25.33	0.90	240.38	$C_{15}H_{28}O_2$
35	3-(azepan-1-yl)-1,2-benzothiazole-1,1-dioxide	26.00	0.17	264.35	$C_{13}H_{16}N_2O_2S$
36	Squalene	26.47	4.57	410.72	$C_{30}H_{50}$
37	Trans-13-Octadecenoic acid	27.17	1.03	282.46	$C_{18}H_{34}O_2$
38	Hexacosane	27.94	0.90	366.71	$C_{26}H_{54}$
39	Selinene	28.45	1.05	204.35	$C_{15}H_{24}$
40	2(1*H*)-Naphthalenone, octahydro-4a-methyl-7-(1-methyl-ethyl)-, (4a. alpha.,7. beta.,8a. beta.)-	28.49	0.08	208.34	$C_{14}H_{24}O$
41	Caparratriene	28.52	0.22	206.37	$C_{15}H_{26}$
42	(2,2,6-trimethylbicyclo [4.1.0] hept-1-yl) methanol	28.59	0.09	168.28	$C_{11}H_{20}O$
43	Ergost-25(27)-ene-3,5,6,12-tetrol	28.63	0.25	448.7	$C_{28}H_{48}O_4$
44	1-Chlorononadecane	32.62	1.66	302.97	$C_{19}H_{39}Cl$

RT= Retention time, MW= Molecular weight

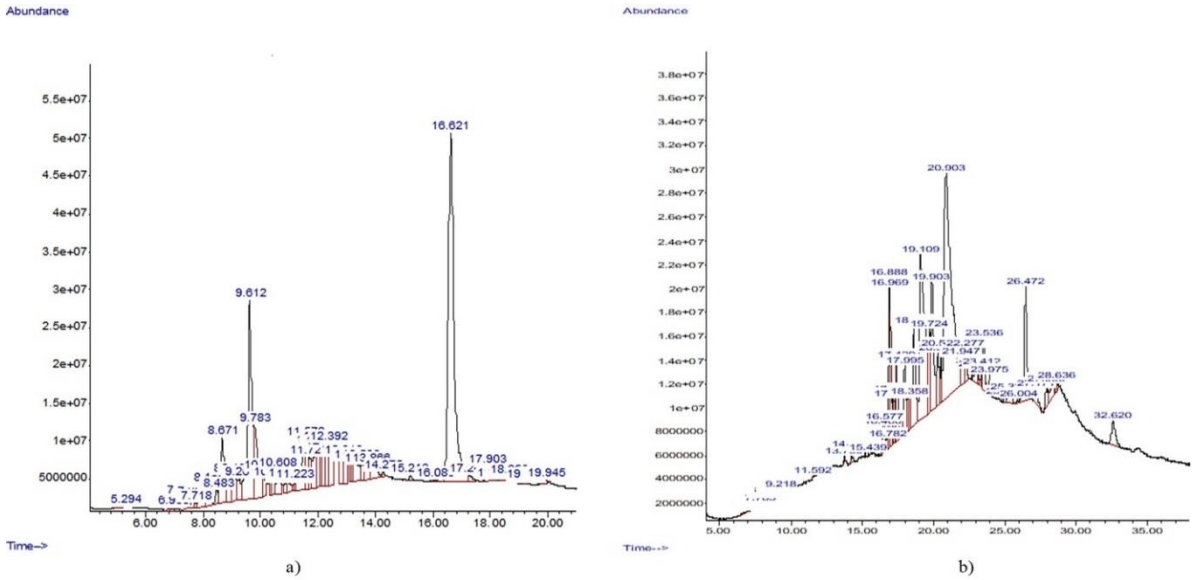

Figure 3. GC-MS chromatogram of compounds identified in the: a) EEF and b) AQF of DM

Antioxidant Potential

TAC

Figure 4 presents the AA calibration curve (a) and the AAE of the TAC of CR, EEF, and AQF of DM (b). At 300 µg/ml, the CR exhibited a significantly ($p < 0.05$) higher TAC (73.59 ± 0.011 µg/ml AAE) than EEF (41.28 ± 0.003 µg/ml AAE) and AQF (31.28 ± 0.005 µg/ml AAE). Furthermore, the EEF and AQF were not significantly different ($p > 0.05$) from each other.

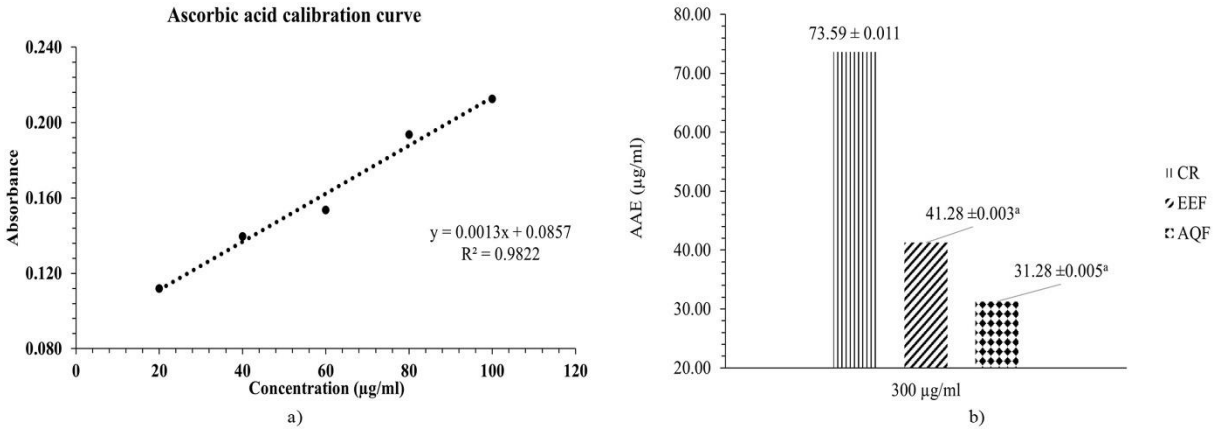

Figure 4. TAC of DM: a) AA calibration curve and b) AAE TAC of DM. Values with [a] superscript are significantly ($p < 0.05$) lower than CR

AA used as a standard in the determination of the antioxidant effect demonstrated a concentration-dependent absorbance yielding a standard calibration curve (Figures 4a and 5a). All the tested samples (CR, EEF, and AQF) exhibited lower total antioxidant capacity compared to AA. This is not surprising considering AA is a standard water-soluble antioxidant and the test medium was polar [50]. The CR extract demonstrating significantly higher total antioxidant capacity might be attributed to the synergistic and additivity properties of phytochemicals [51,52] as some compounds present in the EEF were absent in AQF. Therefore, their combined presence in the CR showed a higher total antioxidant capacity.

TRP

The AA calibration curve (a) and the AAE of the TRP of CR, EEF, and AQF (b) are presented in Figure 5. At 100 µ/ml, the AQF showed a significantly ($p < 0.05$) higher TRP (106.84 ± 3.46 µg/ml AAE) than the CR (93.23 ± 5.63 µg/ml AAE) and EEF (92.35 ± 6.96 µg/ml AAE). However, the CR and EEF were not significantly ($p > 0.05$) different from each other.

The AQF exhibited a slightly higher TRP than AA but significantly ($p < 0.05$) higher than CR and EEF. The TRP of a compound is due to its electron-donating ability [53]. The superior reducing power of the AQF might be attributed to the presence of compounds with high electron-donating potential in the AQF. Although these compounds might be present in the CR, the antagonist effects [52] of some compounds present in the CR but absent in AQF might negatively impact the antioxidant activity of the CR.

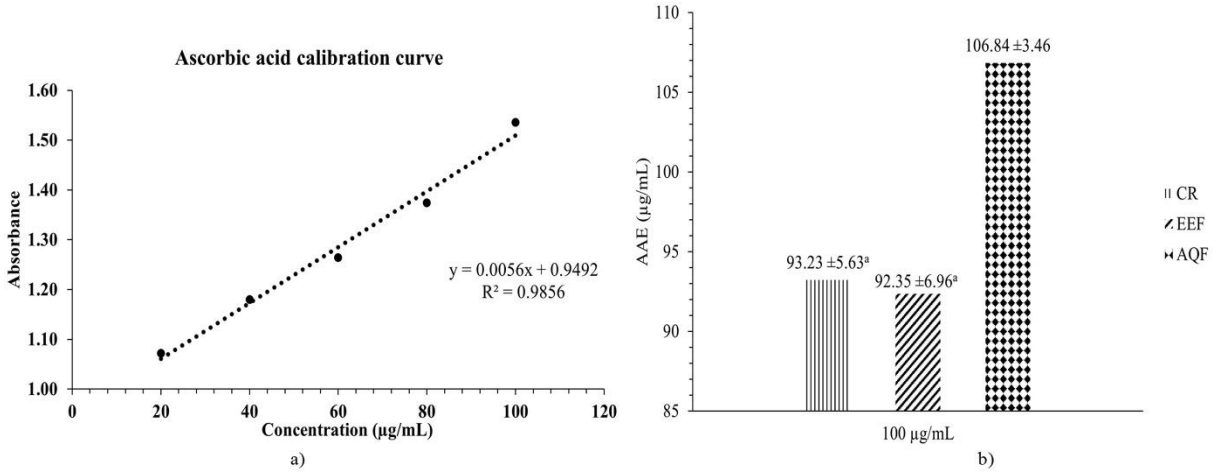

Figure 5. TRP of DM: a) AA calibration curve and b) AAE total reducing power of DM. Values with [a]superscript are significantly ($p < 0.05$) lower than AQF

FTC

The antioxidant capacity of CR, EEF, and AQF expressed by the FTC method is presented in Figure 6a. At 1 mg/ml, the EEF demonstrated a significantly ($p < 0.05$) higher inhibition (48.38% ±4.61) than ascorbic acid (32.64% ±4.40), CR (18.39% ±3.80), and AQF (11.23% ±3.66) in the final day of the experiment (day 6).

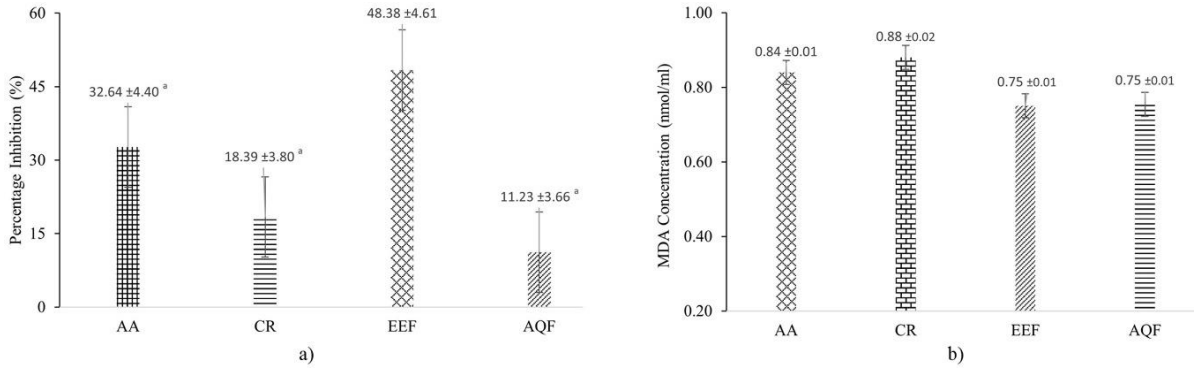

Figure 6. Antioxidant capacity of DM expressed by: a) FTC and b) TBA methods. Values with [a] superscript are significantly ($p < 0.05$) lower than EEF

TBA

The antioxidant potential of CR, EEF, and AQF expressed by the TBA method is shown in Figure 6b. At 1 mg/ml, the EEF and AQF demonstrated lower MDA concentration (0.75 ±0.01 nmol/ml) than the CR (0.88 ±0.02 nmol/ml) and AA (0.84 ±0.01 nmol/ml) on day 6, similar to the result observed for EEF in the FTC method.

H_2O_2 Scavenging Assay

Figure 7 presents the H_2O_2 scavenging activity of CR, EEF, and AQF. The AQF demonstrated significantly ($p < 0.05$) higher (82.72% ±1.88) scavenging at the 20 µg/ml concentration than AA (51.52% ±2.43), CR (33.33% ±2.16), and EEF (63.64% ±2.66). Furthermore, the AQF demonstrated significantly ($p < 0.05$) higher scavenging compared to the CR and EEF at 60, 80, and 100 µg/ml concentrations, with no significant ($p > 0.05$) difference with AA at 100 µg/ml concentration.

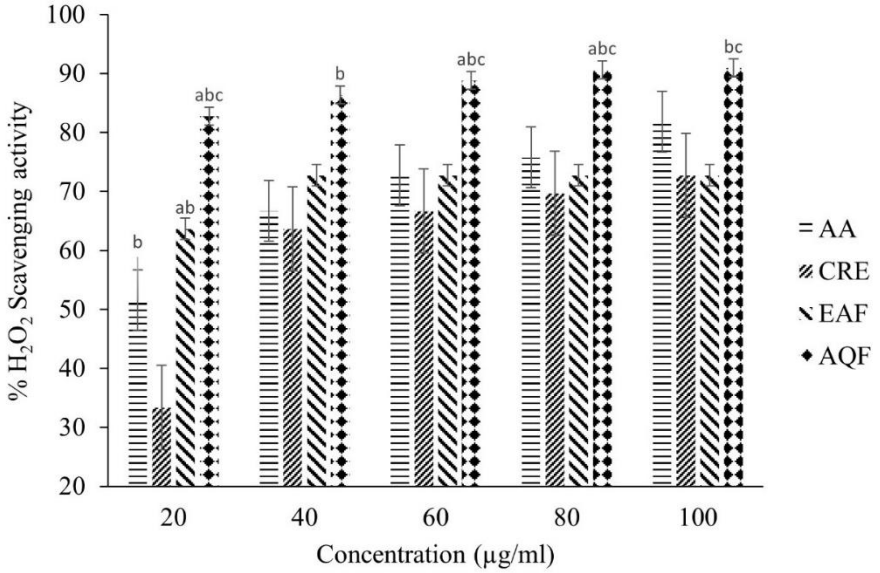

Figure 7. H_2O_2 scavenging activity of DM. Values with [a], [b], and [c] superscripts are significantly ($p < 0.05$) higher than AA, CR, and EEF, respectively

In the FTC method, the early stage of lipid peroxidation due to the production of peroxides is considered. Here, the peroxides combine with ferrous chloride yielding ferric ions which subsequently react with ammonium thiocyanate to produce the red-colored ferric thiocyanate [54]. The prevention of the formation of the red product by the samples is exploited here. Thus, a lower absorbance value translates to higher anti-peroxidation potential. In our study, the EEF exhibited the highest inhibition and lowest MDA concentration demonstrating a significantly higher anti-peroxidation capacity than all the extracts and ascorbic acid. The superiority of the EEF against ascorbic acid in the FTC method might be due to the weak antioxidant capacity of ascorbic acid in a non-polar medium [50] and the semi-polar nature of ethyl acetate. A similar observation was made in the TBA method with ethyl acetate demonstrating the lowest MDA concentration after day 6. The high antioxidant activity observed at the beginning of the experiment which diminished continuously for AA and CR demonstrated powerful anti-lipid peroxidation. However, the EEF and AQF demonstrated a longer antioxidant potential and, thus, a better anti-peroxidation activity. In the hydrogen peroxide scavenging method, the AQF exhibited the highest scavenging ability, significantly higher than the CR and EEF. This further justifies the high reducing power of the AQF reported earlier (Figure 5).

Persistent hyperglycemia associated with diabetes promotes oxidative stress over time *via* reactive oxygen species (ROS) generation and the depletion of the inherent antioxidant system [55]. Some of the problems encountered with antioxidants are storage instability and poor solubility [55] as

revealed by the poor performance of AA in the FTC and TBA method. Furthermore, lipid peroxidation due to persistent hyperglycemia is a major concern in diabetes [56]. Thus, the antioxidant activity demonstrated by CR, EEF, and AQF might contribute to the antidiabetic activity of DM by ameliorating oxidative stress.

In silico Study

MD and MDS

Antioxidant Activity

Table 6 exhibits the results of the docking interactions of XO with the top 10 compounds. Compound VII exhibited the least BA (-8.8 kcal/mol) and Ki (0.35μM) next to XI with respective BA and Ki of -7.4 kcal/mol and 3.71 μM. Moreover, VII exhibited a superior number of HBs (3) than XI (2) though the latter had more HBIs (11). The low BA, Ki, and higher HBs of VII might contribute to a stable and more favorable dock pose than the other compounds as lower BA translates to an energy-favorable docked complex. The BA defines an inverse of the strength and level of interaction between a macromolecule (target) and the ligand (small molecule or compound) [57] while the Ki defines the inhibition constant. XO is a crucial enzyme in the metabolism of purine and catalyzes the rate-limiting step [56]. However, it is linked to oxidative stress by utilizing oxygen as an electron acceptor rather than NAD^+ yielding superoxide anions free radical and other ROS [59]. Thus, the favorable binding of compound VII might affect the enzyme activity and minimize its effects. Moreover, Figure 8a shows the 2D and 3D docking interactions of XO with compounds VII and XI. The MDS result is shown in Figure 8b depicting the chain and residue displacement indicating hinge regions with higher displacement notably between residues 995 to 1028. Thus, further revealing the flexibility of the complex and possible XO inhibition. Additionally, high XO activity was reported to be associated with type 2 diabetes [60]. Therefore, a decrease in its activity might be associated with antidiabetic activity *via* alleviation of oxidative stress.

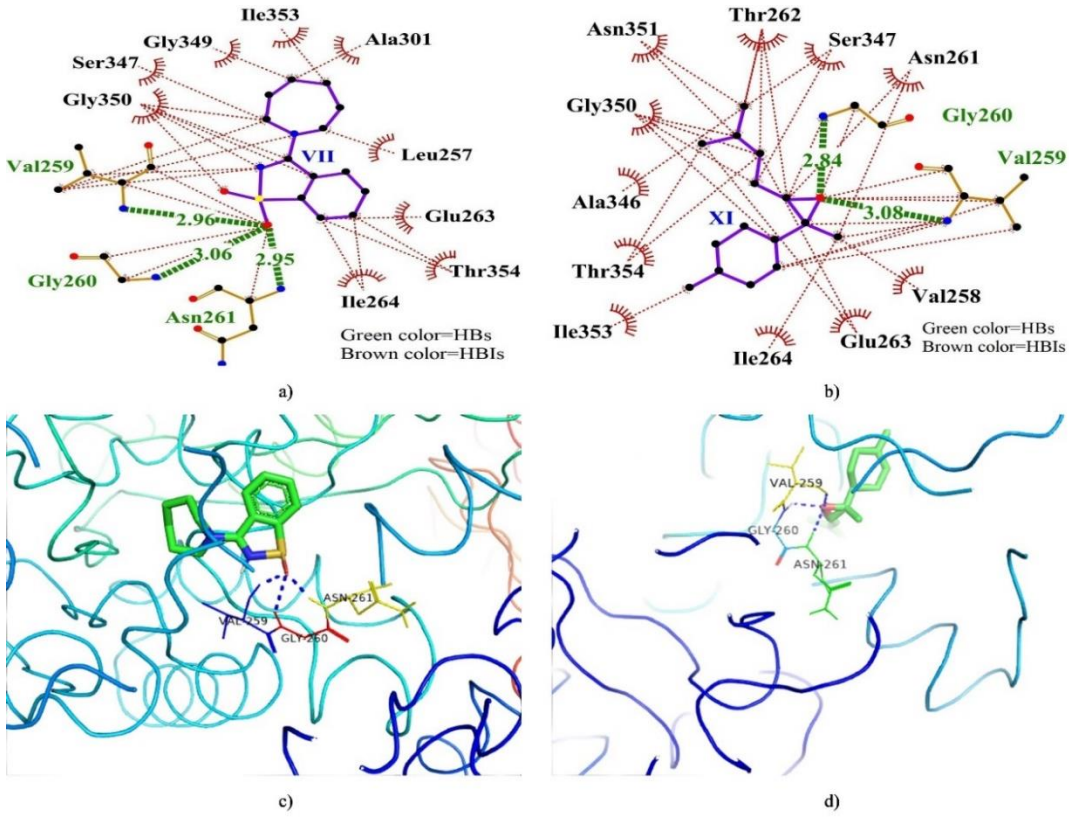

Figure 8a. Docked complex of XO with compounds VII (a and c) and XI (b and d)

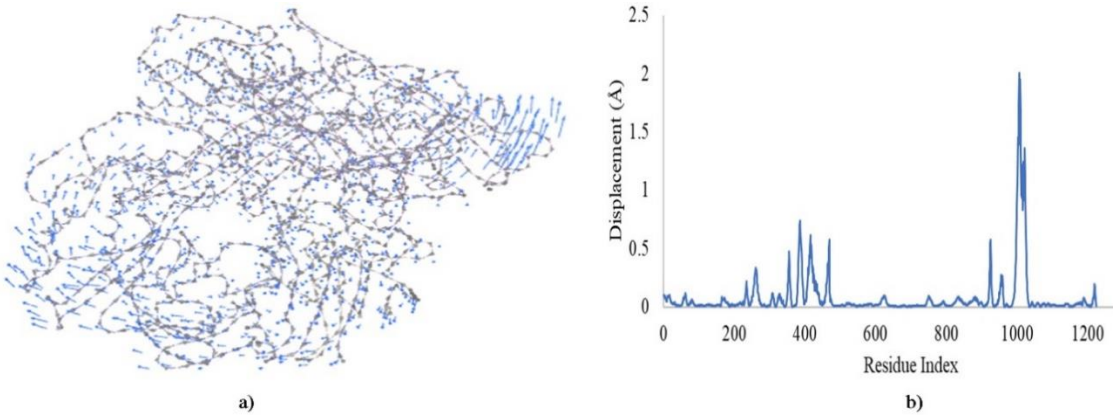

Figure 8b. MDS result of docked XO showing; a) cluster and b) residue displacements

Table 6. Docking interactions of XO with compounds VII and XI

Compounds	Binding Affinity (kcal/mol)	Ki (µM)	Hydrogen Bonds	Hydrophobic Interactions
VII	-8.8	0.35	3	9
XI	-7.4	3.71	2	11
X	-6.7	12.12	0	8
III	-6.5	16.99	1	6
XII	-6.5	16.99	0	8
XIV	-6.4	20.12	1	12
VIII	-6.2	28.20	0	8
VI	-5.9	46.82	3	10
XIII	-5.8	55.44	2	7
XVI	-5.7	65.65	3	8

Table 7 displays the docking interactions of CytP450 21A2 with the compounds. Compound X displayed the lowest BA (-8.5 kcal/mol) and Ki (0.58µM) next to XII with BA and Ki of -8.3 kcal/mol and 0.81 µM, respectively. However, XII exhibited a superior number of HBs (4) with slightly lower HBIs (8). Additionally, compounds VII and IV participated in SB (ASP288) and π-cationic (TRP202) interactions, respectively. Moreover, Figure 9a shows the interactions of CytP450 21A2 with compounds X and XI depicting the residues participating in both HBs and HBIs interactions. CytP450 21A2 belongs to the heme monooxygenases family with their activities associated with the generation of ROS by uncoupled catalytic action [61]. Thus, in ailments associated with depletion of the inherent antioxidant system such as diabetes, inhibition leading to its decreased activity might contribute to decreased oxidative stress.

Table 7. Docking interactions of CytP450 21A2 with compounds VII and XI

Compounds	Binding Affinity (kcal/mol)	Ki (µM)	Hydrogen Bonds	Hydrophobic Interactions	Salt Bridge	π-Stacking
X	-8.5	0.58	0	10		
XII	-8.3	0.81	4	8		
VII	-8.2	0.96	1	8	ASP288	
III	-7.9	1.60	1	9		
XII	-7.5	3.14	1	11		
VIII	-7.2	5.21	0	9		
I	-6.9	8.64	4	5		
XIV	-6.9	8.64	4	7		
XIII	-6.5	16.99	3	8		
IV	-6.4	20.12	0	4		TRP202

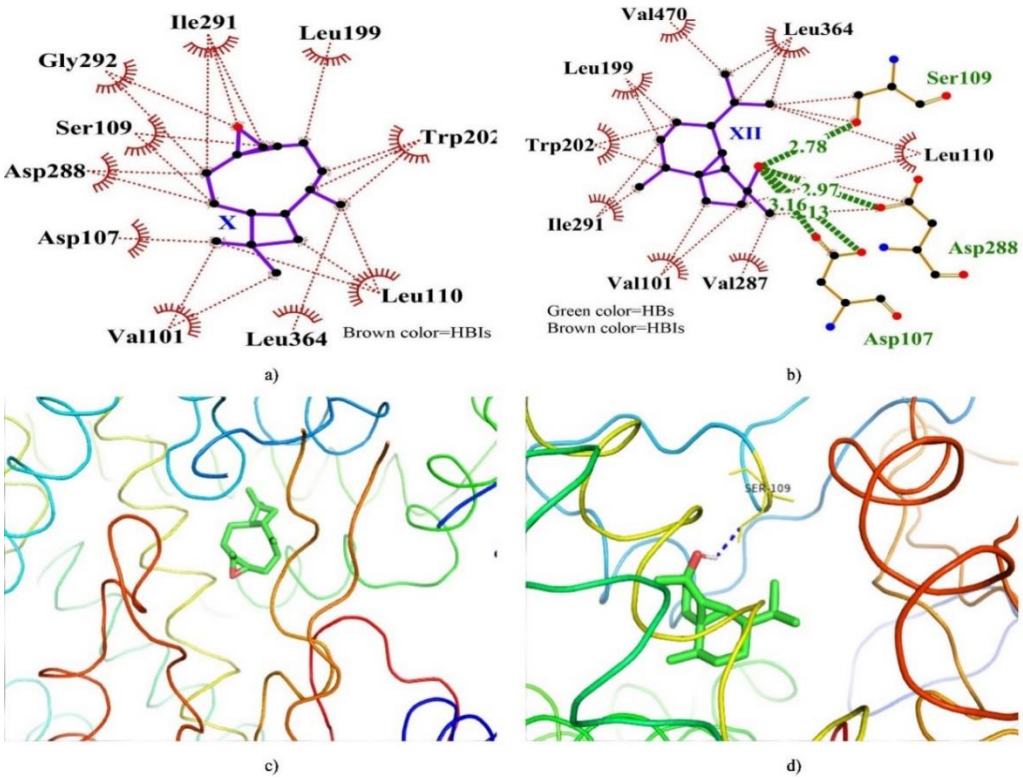

Figure 9a. Docked complex of CytP450 21A2 with compounds X (a and c) and XII (b and d)

Furthermore, the MDS result of the docked CytP450 21A2 complex is exhibited in Figure 9b showing high cluster and residue displacements (3.343 Å) close to the mid-chain residues which might disrupt its tertiary structure and its activity.

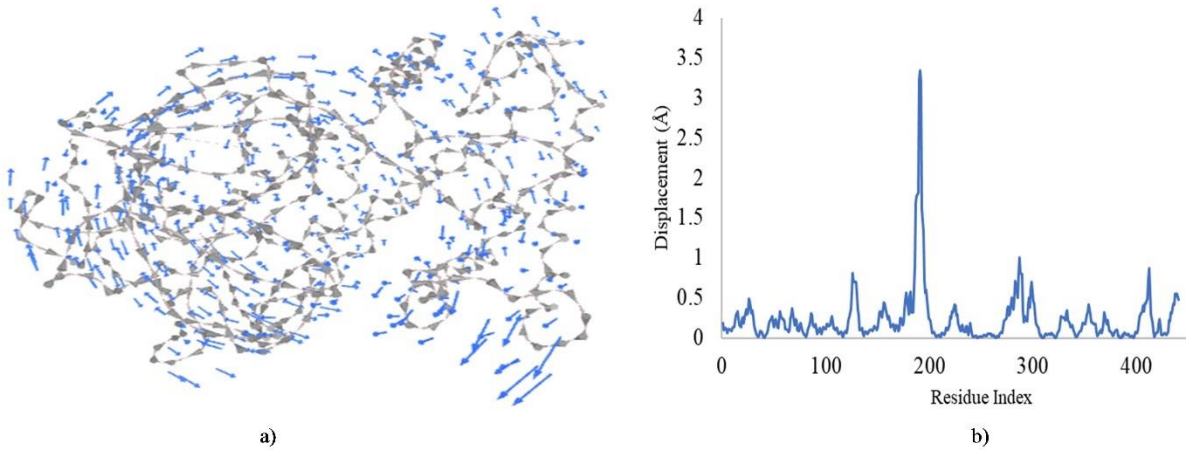

Figure 9b. MDS result of docked CytP450 21A2 showing; a) cluster and b) residue displacements

Table 8 reveals the docking interactions of NOX with the compounds. The lowest BA (-8 kcal/mol) and Ki (1.35µM) were demonstrated by compound VII followed by III with respective BA and Ki of -6.9 kcal/mol and 8.64 µM. Higher interaction was also observed for VII with a superior number of HBs and HBIs than the other compounds including an SB formed with GLU32. Moreover, compounds III, VIII, and XIII were involved in SB formation with GLU32, GLU32, and HIS10, respectively. NOX are groups of membrane-bound proteins transferring electrons across the membrane

to oxygen-generating superoxide anions and ROS such as the hydroxyl and H_2O_2 radicals [62]. Thus, in a state of impaired body antioxidant systems such as diabetes, ROS accumulate. Decreased activity of this enzyme in these ailments might lead to decreased oxidative stress and promote healing.

Table 8. Docking interactions of NOX with compounds VII and III

Compounds	Binding Affinity (kcal/mol)	Ki (μM)	Hydrogen Bonds	Hydrophobic Interactions	Salt Bridge
VII	-8	1.35	2	12	GLU32
III	-6.9	8.64	1	10	
XI	-6.7	12.12	0	12	
XII	-6.6	14.35	3	8	
XIV	-6.3	23.82	3	10	
VIII	-6.2	28.20	0	8	GLU32
X	-6.2	28.20	0	10	
XIII	-5.8	55.44	8	3	HIS10
III	-5.6	77.73	1	10	GLU32
IV	-5.6	77.73	0	10	

Figure 10a shows the HBs and HBIs formation by NOX with compounds VII and III depicting a stabilized docked complex. Figure 10b displays the MDS result depicting the cluster and residue displacements with notable displacements at both terminals. However, higher displacements up to 3.385 and 2.285 Å were observed at residues 365 and 426, respectively. This might disrupt the enzyme activity by disrupting its tertiary structure, further indicating a possible inhibition of the enzyme by the compounds.

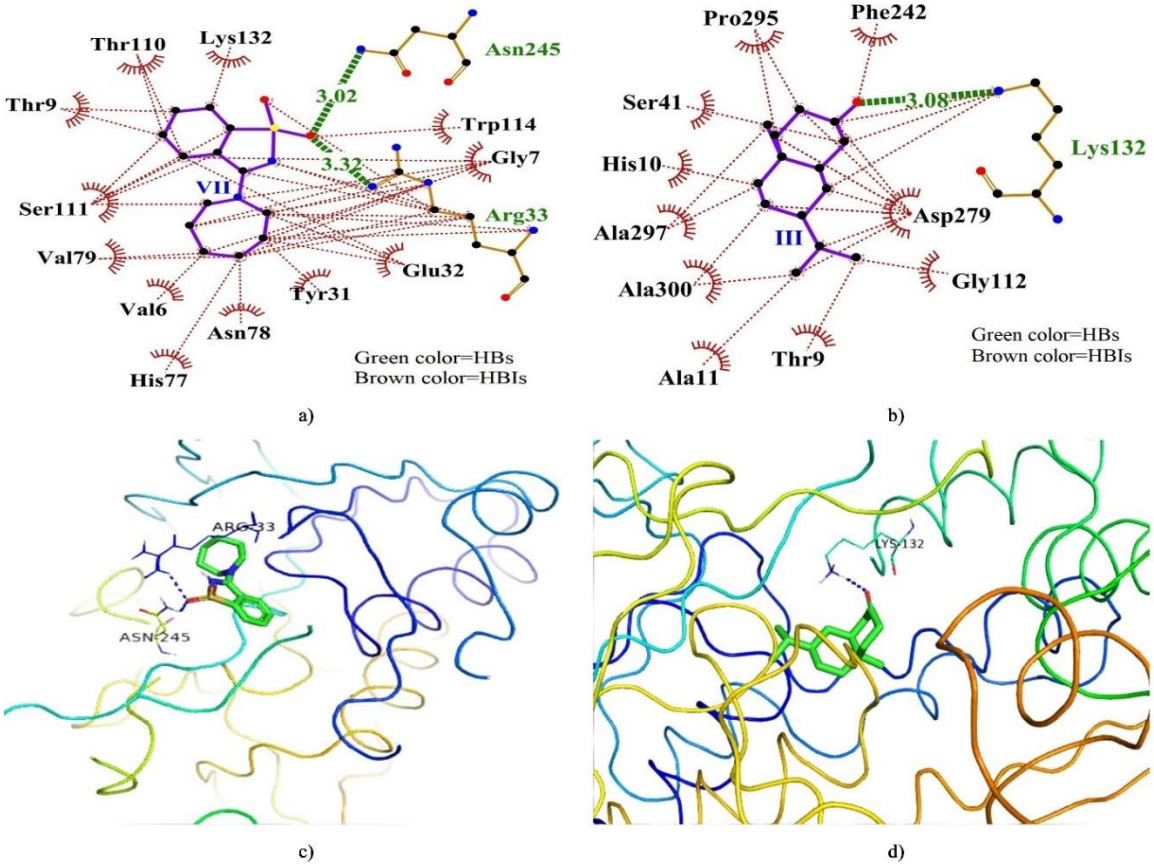

Figure 10a. Docked complex of NOX with compounds VII (a and c) and III (b and d)

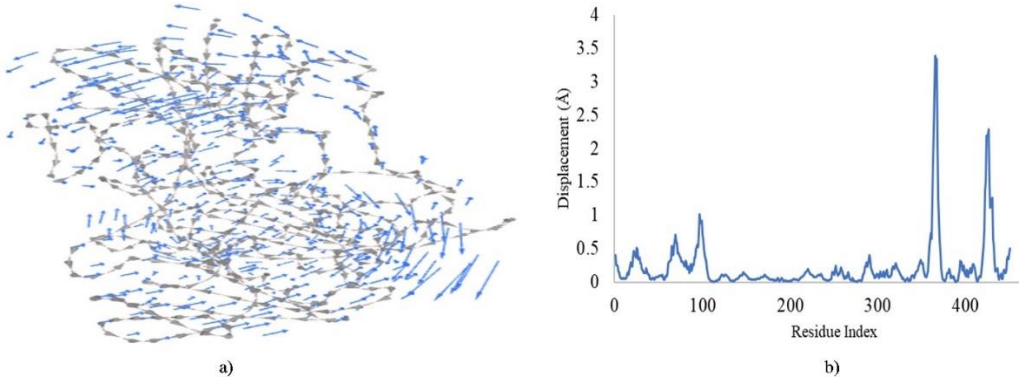

Figure 10b. MDS result of docked NOX showing; a) cluster and b) residue displacements

Antidiabetic Activity

Table 9 reveals the docking interactions of PTP1B with the compounds. Compound III exhibited the lowest BA (-7.5 kcal/mol) and Ki (3.14 µM) slightly lower than X with BA and Ki of -7.4 kcal/mol and 3.71 µM, respectively. Additionally, III exhibited 3 HBs and 7 HBIs, slightly higher and lower than X, respectively.

Figure 11a depicts the docking interactions of PTP1B with compounds III and X revealing the HBs and HBIs. Both compounds formed HBs with ARG221 and SER216 residues. Additionally, the MDS of the docked PTP1B complex is displayed in Figure 11b showing the chain cluster and residue displacements. Notable displacement was observed at 6 regions depicting hinge regions and cluster movements with the highest displacement (2.65 Å) at approximately mid-chain (residue 265).

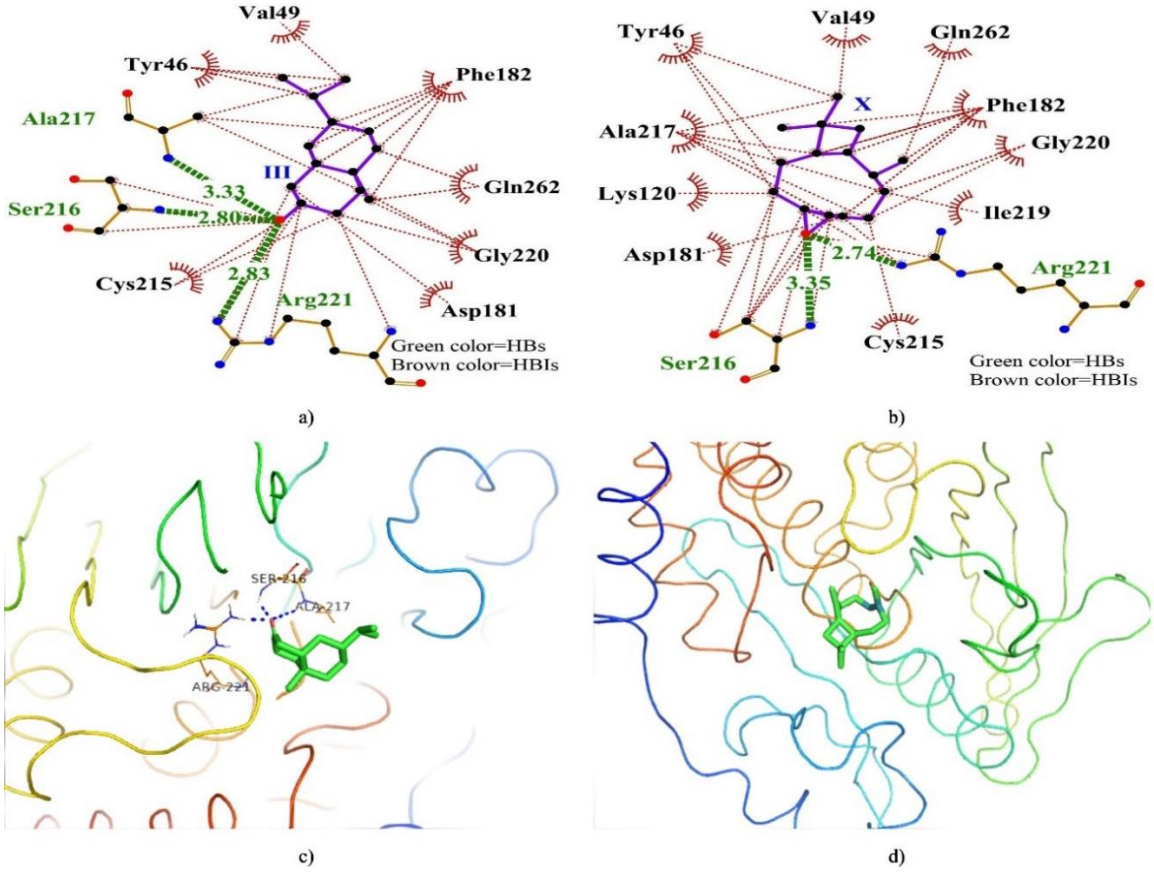

Figure 11a. Docked complex of PTP1B with compounds III (a and c) and X (b and d)

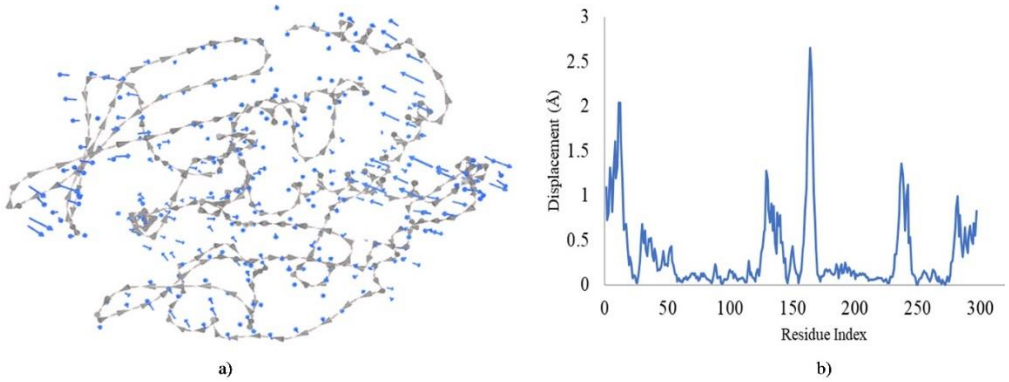

Figure 11b. MDS result of docked PTP1B showing; a) cluster and b) residue displacements

Table 9. Docking interactions of PTP1B with the compounds

Compounds	Binding Affinity (kcal/mol)	Ki (μM)	Hydrogen Bonds	Hydrophobic Interactions	π-Cation	Salt Bridge	Halogen Bond
III	-7.5	3.14	3	7			
X	-7.4	3.71	2	9			
VII	-7.2	5.21	2	7			
XI	-7.2	5.21	0	11			
XIV	-7	7.30	2	11			
VIII	-6.8	10.23	0	7			
XIII	-6.7	12.12	4	8		LYS120 ARG221	
XII	-6.3	23.82	1	10			
IV	-6.2	28.20	1	7	PHE182		LYS120
II	-5.8	55.44	1	8			

PTP1B is an insulin-desensitizing enzyme that downregulates the insulin receptor phosphorylation. Therefore, decreases insulin sensitivity in tissues *via* the insulin signaling pathway and promotes insulin resistance [63]. Inhibition of its activity promotes insulin signaling and absorption of glucose and decreases hyperglycemia. Thus, a promising target of diabetic therapy. In our study, the docking of the top two compounds in the PTP1B active site interacting with the amino acids might block the activity of the enzyme and decrease insulin resistance.

The docking interaction of PPARγ with the compounds is displayed in Table 10 depicting the various binding interactions. Compound X exhibited a slightly lower BA (-8.5 kcal/mol) and Ki (0.58 μM) than XII with a BA and Ki of -8.3 kcal/mol and 0.81 μM, respectively. However, the latter had a higher number of HBs (1) and HBIs (13). Furthermore, these docking interactions are displayed in Figure 12a showing the HBs and HBIs whereas the MDS of the docked PPARγ complex is shown in Figure 12b depicting the cluster and residue displacement.

Table 10. Docking interactions of PPARγ with the compounds

Compounds	Binding Affinity (kcal/mol)	Ki (μM)	Hydrogen Bonds	Hydrophobic Interactions
X	-8.5	0.58	0	6
XII	-8.3	0.81	1	13
VII	-8.2	0.96	1	10
III	-7.9	1.60	0	6
XII	-7.5	3.14	0	14
VIII	-7.2	5.21	0	12
I	-6.9	8.64	1	6
XIV	-6.9	8.64	3	10
XIII	-6.5	16.99	1	14
IV	-6.4	20.12	0	8

PPARγ is part of the nuclear hormone receptors family acting as ligand-modulated transcription factors that regulate lipid metabolism by simulating insulin sensitivity, proliferation, and cell differentiation [64]. These receptors have emerged as antidiabetic drug targets, notably the thiazolidinediones which lower insulin resistance and improve glycemic control [64]. In our study, compounds X and XII interacted with PPARγ with low BA and Ki in the thiazolidinediones binding pocket which might its activity and improve insulin resistance.

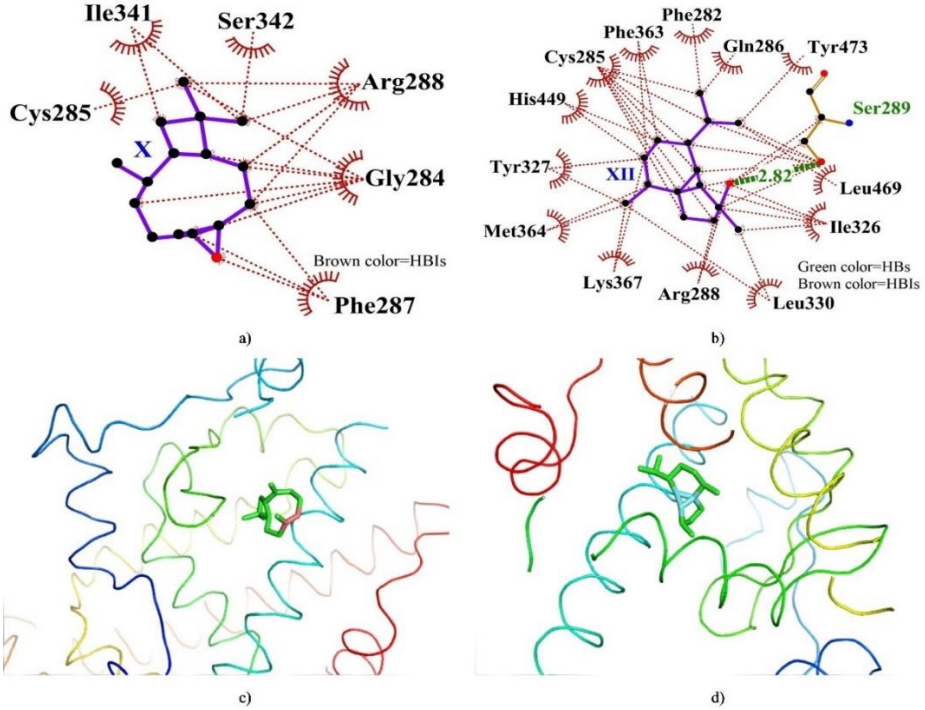

Figure 12a. Docked complex of PPARγ with compounds X (a and c) and XII (b and d)

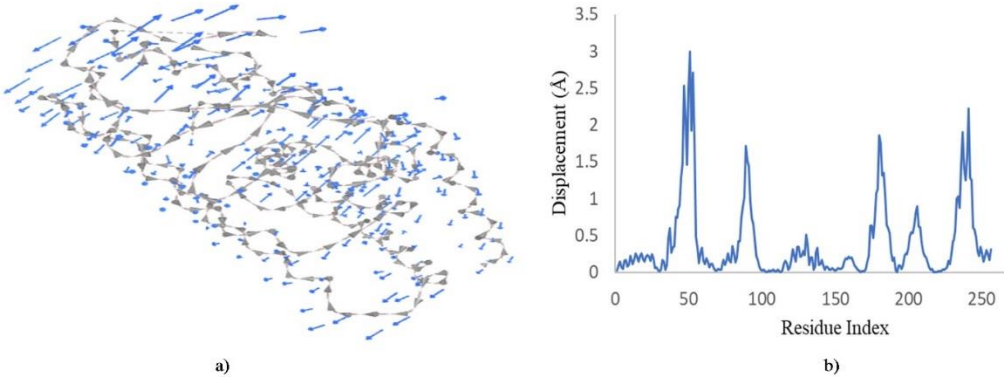

Figure 12b. MDS result of docked PPARγ showing; a) cluster and b) residue displacements

The ADMET predictions of the top two compounds with the least BA and Ki are displayed in Table 11. Compound VII was predicted to be slightly soluble (-2.87 log mol/L) while the others were insoluble with III (-4.98 log mol/L) being the least. However, the compounds were predicted to have high human intestinal absorption with compound X (95.88%) demonstrating the highest percentage of absorption while VII (94.24%) was the least. Furthermore, compounds VII (-3.60 log Kp), X (-3.07 log Kp), and XI (-3.27 log Kp) were predicted to be skin permeant while III and XII were relatively less permeant. Moreover, the compounds were predicted to be neither inhibitors of P-glycoproteins nor its

substrate. For a compound to exert pharmacological effects, it must be effectively absorbed and remain bioavailable for a while which also contributes to safe usage and predicts its onset and intensity [65]. In our study, some of the compounds were predicted to possess good absorption properties.

Table 11. ADMET properties of the compounds

ADMET Properties		**III**	**VII**	**X**	**XI**	**XII**
Absorption	Water solubility (log mol/L)	-4.98	-2.87	-4.42	-4.60	-4.55
	Human Intestinal absorption (%)	95.10	94.24	95.88	95.29	94.86
	Skin permeability (log Kp)	-1.76	-3.60	-3.07	-3.27	-2.23
	P-glycoprotein substrate	No	No	No	No	No
	P-glycoprotein I inhibitor	No	No	No	No	No
	P-glycoprotein II inhibitor	No	No	No	No	No
Distribution	The volume of distribution [VDss (log L/kg)]	0.45	0.01	0.59	0.53	0.55
	Human fraction unbound	0.21	0.26	0.33	0.33	0.19
	BBB permeability (log BB)	0.64	0.31	0.65	0.67	0.68
	CNS permeability (log PS)	-1.75	-2.85	-2.52	-2.57	-1.97
Metabolism	CYP2D6 substrate	No	No	No	No	No
	CYP3A4 substrate	Yes	No	No	No	Yes
	CYP1A2 inhibitor	No	No	Yes	No	Yes
	CYP2C19 inhibitor	No	No	Yes	Yes	Yes
	CYP2C9 inhibitor	No	No	Yes	No	No
	CYP2D6 inhibitor	No	No	No	No	No
	CYP3A4 inhibitor	No	No	No	No	No
Excretion	Total clearance (log ml/min/kg)	1.05	0.33	0.91	1.24	0.89
	Renal OCT2 substrate	No	No	No	No	No
Toxicity	Human max. tolerated dose (log mg/kg/day)	-0.21	0.12	0.19	0.22	-0.32
	hERG I inhibitor	No	No	No	No	No
	hERG II inhibitor	No	No	No	No	No
	LD_{50} [rats (mol/kg)]	1.56	2.68	1.55	1.48	1.69
	Hepatotoxicity	No	Yes	No	No	No
	Skin sensation	Yes	No	Yes	Yes	Yes

Compound X was predicted to have a higher (0.59 log L/kg) steady-state volume of distribution (VDss) than the others with the lowest VDss exhibited by VII (0.01 log L/kg). The VDss predicts the amount of the compound required to be equally distributed between tissues and plasma with higher values (log VDss > 0.45) indicating higher concentration in tissues while values < -0.15 and > 0.45 are considered low [31]. Thus, in our study, the compounds had higher VDss. Furthermore, X and XI had similar fraction unbound values (0.33) while XII had the lowest value (0.19). Compounds XII, XI, X, and III exhibited similar BBB (blood-brain barrier) permeability properties in order of decreasing values (0.69-0.64 log BB) while VII had the lowest (0.31 log BB). The log BB value accounts for the crossing of the BBB which determines brain toxicity and side effects as a log ratio of brain-plasma drug concentration [31]. In our study, the compounds were predicted to be BBB permeant. Moreover, VII showed the lowest (-2.85 log PS) CNS (central nervous system) permeability next to XI (-2.57 log PS) and X (-2.52 log PS) while III (-1.75 log PS) had the highest. A CNS permeability value (log PS) >-2 is considered CNS permeant while < -3 is not. Thus, the compounds were predicted to be CNS permeant in our study.

All the compounds were predicted to be non-CYP2D6 substrates but III and XII were CYP3A4 substrates. X and XII were CYP1A2 and CYP2C19 inhibitors while XI inhibited only the latter. Additionally, X was predicted to be a CYP2C9 inhibitor while none were CYP2D6 and 3A4 inhibitors. CytP450 is associated with the metabolism and subsequent excretion of many compounds and their inhibitors can alter their effects on drugs [31]. CYP2D6 and CYP3A4 metabolize many compounds. In our study, compounds III and XII were predicted to be metabolized by these enzymes while VII was neither a substrate nor inhibitor of the cytP450 enzymes. Compound XI had the highest (1.24 log ml/min/kg) total clearance rate next to III (1.05 log ml/min/kg) while VII (0.33 log ml/min/kg) had the

lowest. Additionally, all the compounds were not renal OCT2 (organic cation transporter 2) substrates. The renal OCT2 is crucial in the clearance and disposition of drugs in the kidney [31], thus, the compounds can easily undergo renal clearance and disposition.

Compounds X (0.19 log mg/kg/day) and XI (0.22 log mg/kg/day) were predicted to have slightly different maximum tolerable doses in humans while XIII had the lowest (-0.32 log mg/kg/day). A maximum tolerated dose < 0.477 log (mg/kg/day) is considered low while above the value is high [31]. Thus, the compounds were within the low range. Moreover, the compounds were predicted not to be hERG I and II inhibitors. Compound VII has the highest (2.68 mol/kg) LD50 value while III (1.56 mol/kg), X (1.55 mol/kg), and XI (1.48 mol/kg) had slightly different values though the latter had the lowest. Compound VII was predicted to be hepatotoxic, however, it's the only one predicted not to exert skin sensation.

In our study, the antioxidant and antidiabetic potential of DM leaf was explored by investigating its secondary metabolites, antioxidant, and antidiabetic activity. Among the compounds, 3-(azepan-1-yl)-1,2-benzothiazole 1,1-dioxide and caryophyllene oxide were the most antioxidant compounds. This isn't surprising considering their high abundance in the EEF which exhibited the highest anti-peroxidation by the FTC and TBA methods. Thus, there is a correlation between the *in vitro* and *in-silico* results. Moreover, 3-(azepan-1-yl)-1,2-benzothiazole 1,1-dioxide showed good drug candidacy predicted by the ADMET study. For the antidiabetic activity, caryophyllene oxide was identified as the most antidiabetic compound next to 4a-methyl-7-(propan-2-yl) octahydronaphthalen-2(1H)-one. Although the present study showed the antioxidant, antidiabetic, and ADMET of these compounds, further studies such as isolation and *in vivo* antioxidant and antidiabetic studies of the compounds will further document these properties. Additionally, structural modification of the compounds might enhance the ADMET properties of the compounds. Conclusively, DM contains several compounds that might be associated with the antioxidant and antidiabetic activity of the plant due to the observed scavenging and the *in-silico* antioxidant, antidiabetic, and ADMET study. Additionally, all the extracts possess significant antioxidant activity and some of the identified compounds might be novel sources of antioxidant and antidiabetic drugs.

ACKNOWLEDGEMENTS

The authors express their immense gratitude to the Tertiary Education Fund of Nigeria for the research sponsorship *via* the Institutional Based Research Fund. Additionally, the institutional support of the Department of Pharmaceutical Technology, Adamawa State Polytechnic Yola is duly acknowledged.

AUTHOR CONTRIBUTIONS

Concept: M.M.D., N.M.; Design: M.M.D., N.M.; Control: M.M.D., N.M.; Sources: M.M.D.; Materials: M.M.D., N.M.; Data Collection and/or Processing: M.M.D., N.M.; Analysis and/or Interpretation: M.M.D., N.M.; Literature Review: M.M.D.; Manuscript Writing: M.M.D.; Critical Review: M.M.D., N.M.; Other: -

CONFLICT OF INTEREST

The authors declare that there is no real, potential, or perceived conflict of interest for this article.

ETHICS COMMITTEE APPROVAL

The authors declare that the ethics committee approval is not required for this study.

REFERENCES

1. American Diabetes Association. (2020). Pharmacologic Approaches to Glycemic Treatment: Standards of Medical Care in Diabetes-2020. Diabetes Care, 43(Supplement_1), S98-S110. [CrossRef]
2. American Diabetes Association Professional Practice Committee. (2022). Classification and Diagnosis of Diabetes: Standards of Medical Care in Diabetes-2022. Diabetes Care, 45(Supplement_1), S17-S38.

[CrossRef]
3. Dahiru, M.M. Samuel, N.M. (2022). A review of the mechanisms of action and side effects of anti-diabetic agents. Trends in Pharmaceutical Sciences, 8(3), 195-210. [CrossRef]
4. Ogurtsova, K., Guariguata, L., Barengo, N.C., Ruiz, P.L.D., Sacre, J.W., Karuranga, S., Sun, H., Boyko, E. J. Magliano, D.J. (2022). IDF diabetes Atlas: Global estimates of undiagnosed diabetes in adults for 2021. Diabetes Research and Clinical Practice, 183, 109118. [CrossRef]
5. Sun, H., Saeedi, P., Karuranga, S., Pinkepank, M., Ogurtsova, K., Duncan, B.B., Stein, C., Basit, A., Chan, J.C. Mbanya, J.C. (2022). IDF Diabetes Atlas: Global, regional, and country-level diabetes prevalence estimates for 2021 and projections for 2045. Diabetes Research and Clinical Practice, 183, 109119. [CrossRef]
6. Dahiru, M.M. (2023). Recent advances in the therapeutic potential phytochemicals in managing diabetes. Journal of Clinical and Basic Research, 7(1), 13-20.
7. Dahiru, M.M., Badgal, E.B. Neksumi, M. (2023). Phytochemical profiling and heavy metals composition of aqueous and ethanol extracts of Anogeissus leiocarpus. Journal of Faculty of Pharmacy of Ankara University, 47(2), 311-323. [CrossRef]
8. Abdel Motaal, A., Salem, H.H., Almaghaslah, D., Alsayari, A., Bin Muhsinah, A., Alfaifi, M.Y., Elbehairi, S.E.I., Shati, A.A. El-Askary, H. (2020). Flavonol glycosides: in vitro inhibition of dppiv, aldose reductase and combating oxidative stress are potential mechanisms for mediating the antidiabetic activity of cleome droserifolia. Molecules, 25(24), 5864. [CrossRef]
9. Abdou, H.M., Hamaad, F.A., Ali, E.Y. Ghoneum, M.H. (2022). Antidiabetic efficacy of Trifolium alexandrinum extracts hesperetin and quercetin in ameliorating carbohydrate metabolism and activating IR and AMPK signaling in the pancreatic tissues of diabetic rats. Biomedicine and Pharmacotherapy, 149, 112838. [CrossRef]
10. Adhikari, B. (2021). Roles of alkaloids from medicinal plants in the management of diabetes mellitus. Journal of Chemistry, 2021, 1-10. [CrossRef]
11. Amah, C.C., Joshua, P.E., Ekpo, D.E., Okoro, J.I., Asomadu, R.O., Obelenwa, U.C. Odiba, A.S. (2022). Ethyl acetate fraction of Fagara zanthoxyloides root-bark possess antidiabetic property against alloxan-induced diabetes and its complications in Wistar rat model. Journal of Ethnopharmacology, 293, 115259. [CrossRef]
12. An, S., Niu, D., Wang, T., Han, B., He, C., Yang, X., Sun, H., Zhao, K., Kang, J. Xue, X. (2021). Total Saponins Isolated from Corni Fructus via Ultrasonic Microwave-Assisted Extraction Attenuate Diabetes in Mice. Foods, 10(3), 670. [CrossRef]
13. Dahiru, M.M. Nadro, M.S. (2022). Anti-diabetic potential of Hyphaene thebaica fruit in streptozotocin-induced diabetic rats. Journal of Experimental and Molecular Biology, 23(1), 29-36. [CrossRef]
14. Tropical Plants Database. (2023). Diospyros mespiliformis. Retrieved July 24, 2023, from https://tropical.theferns.info/viewtropical.php?id=Diospyros+mespiliformis.
15. Suleiman Abdulhamid, A. Osagye, I. (2021). Medicinal and traditional utilization of african ebony (diospyros mespiliformi): A review. International Journal of Current Microbiology and Applied Sciences, 10, 811-817. [CrossRef]
16. Ahmed, A.H. Mahmud, A.F. (2017). Pharmacological activities of Diospyros mespiliformis: A review. International Journal of Pharmacy and Biological Sciences, 7, 93-96.
17. Evans, W.C. (2009). Trease and Evans' pharmacognosy: Elsevier Health Sciences, Amsterdam, p.378.
18. Dahiru, M.M., Badgal, E.B. Musa, N. (2022). Phytochemistry, GS-MS analysis, and heavy metals composition of aqueous and ethanol stem bark extracts of *Ximenia americana*. GSC Biological and Pharmaceutical Sciences, 21(3), 145-156. [CrossRef]
19. Prieto, P., Pineda, M., Aguilar, M. (1999). Spectrophotometric quantitation of antioxidant capacity through the formation of a phosphomolybdenum complex: Specific application to the determination of vitamin E. Analytical Biochemistry, 269(2), 337-341. [CrossRef]
20. Oyaizu, M. (1986). Studies on products of browning reaction antioxidative activities of products of browning reaction prepared from glucosamine. The Japanese Journal of Nutrition and Dietetics, 44(6), 307-315. [CrossRef]
21. Kikuzaki, H., Nakatani, N. (1993). Antioxidant effects of some ginger constituents. Journal of Food Science, 58(6), 1407-1410. [CrossRef]
22. Sannigrahi, S., Mazuder, U.K., Pal, D.K., Parida, S. Jain, S. (2010). Antioxidant potential of crude extract and different fractions of Enhydra fluctuans Lour. Iranian journal of pharmaceutical research: IJPR, 9(1), 75. [CrossRef]
23. Kwon, T.W. Watts, B. (2006). Determination of malonaldehyde by ultraviolet spectrophotometry. Journal of Food Science, 28, 627-630. [CrossRef]

24. Zhang, X.Y. (2000). Principles of chemical analysis. Beijing: China Science Press, 275, 276.
25. Sanner, M.F. (1999). Python: A programming language for software integration and development. Journal of Molecular Graphics and Modelling, 17(1), 57-61.
26. Jendele, L., Krivák, R., Škoda, P., Novotný, Hoksza, M.D. (2019). PrankWeb: A web server for ligand binding site prediction and visualization. Nucleic Acids Research, 47(W1), W345-W349. [CrossRef]
27. Laskowski, R.A. Swindells, M.B. (2011). Ligplot+: multiple ligand–protein interaction diagrams for drug discovery. Journal of Chemical Information and Modeling, 51(10), 2778-2786. [CrossRef]
28. Adasme, M.F., Linnemann, K.L., Bolz, S.N., Kaiser, F., Salentin, S., Haupt, V.J. Schroeder, M. (2021). PLIP 2021: Expanding the scope of the protein-ligand interaction profiler to DNA and RNA. Nucleic Acids Research, 49(W1), W530-W534. [CrossRef]
29. Tiwari, S.P., Fuglebakk, E., Hollup, S.M., Skjærven, L., Cragnolini, T., Grindhaug, S.H., Tekle, K. M.Reuter, N. (2014). WEBnm@ v2.0: Web server and services for comparing protein flexibility. BMC Bioinformatics, 15(1), 427. [CrossRef]
30. Ortiz, C.L.D., Completo, G.C., Nacario, R.C., Nellas, R.B. (2019). Potential inhibitors of galactofuranosyltransferase 2 (GlfT2): Molecular docking, 3D-QSAR, and *in silico* ADMETox studies. Scientific Reports, 9(1), 17096. [CrossRef]
31. Pires, D.E.V., Blundell, T.L., Ascher, D.B. (2015). pkCSM: Predicting small-molecule pharmacokinetic and toxicity properties using graph-based signatures. Journal of Medicinal Chemistry, 58(9), 4066-4072. [CrossRef]
32. Mohammed Junaid Hussain, D., Sathish Kumar, K., Darul Raiyaan, G.I., Mohamed Khalith, S.B., Sundarapandian, S. Kantha Deivi, A. (2020). Effect of solvents on phytochemical composition and antioxidant activity of *Cardiospermum halicacabum* (l.) extracts. Pharmacognosy Journal, 12(6), 1241-1251. [CrossRef]
33. Sharma, S., Kumari, A., Dhatwalia, J., Guleria, I., Lal, S., Upadhyay, N., Kumar, V. Kumar, A. (2021). Effect of solvents extraction on phytochemical profile and biological activities of two Ocimum species: A comparative study. Journal of Applied Research on Medicinal and Aromatic Plants, 25, 100348. [CrossRef]
34. Thouri, A., Chahdoura, H., El Arem, A., Omri Hichri, A., Ben Hassin, R. Achour, L. (2017). Effect of solvents extraction on phytochemical components and biological activities of Tunisian date seeds (var. Korkobbi and Arechti). BMC Complementary and Alternative Medicine, 17(1), 248. [CrossRef]
35. Chóez-Guaranda, I., Viteri-Espinoza, R., Barragán-Lucas, A., Quijano-Avilés, M. Manzano, P. (2022). Effect of solvent-solvent partition on antioxidant activity and GC-MS profile of *Ilex guayusa* Loes. leaves extract and fractions. Natural product research, 36(6), 1570-1574. [CrossRef]
36. Basri, A.M., Taha, H. Ahmad, N. (2017). A review on the pharmacological activities and phytochemicals of *Alpinia officinarum* (Galangal) extracts derived from bioassay-guided fractionation and isolation. Pharmacognosy Reviews, 11(21), 43. [CrossRef]
37. Berk, Z. (2018). Food process engineering and technology: Academic press, Massachusetts, p.379.
38. Ebbo, A.A., Sani, D., Suleiman, M.M., Ahmed, A. Hassan, A.Z. (2019). Phytochemical composition, proximate analysis and antimicrobial screening of the methanolic extract of *Diospyros mespiliformis* Hochst Ex a. Dc (Ebenaceae). Pharmacognosy Journal, 11(2), 362-368. [CrossRef]
39. Ebbo, A.A., Sani, D., Suleiman, M.M., Ahmad, A. Hassan, A.Z. (2020). Acute and sub-chronic toxicity evaluation of the crude methanolic extract of Diospyros mespiliformis hochst ex a. Dc (ebenaceae) and its fractions. Toxicology Reports, 7, 1138-1144. [CrossRef]
40. Lozano-Grande, M.A., Gorinstein, S., Espitia-Rangel, E., Dávila-Ortiz, G. Martínez-Ayala, A.L. (2018). Plant sources, extraction methods, and uses of squalene. International Journal of Agronomy, 2018, 1829160. [CrossRef]
41. Kaur, G., Tharappel, L.J.P. Kumawat, V. (2018). Research article evaluation of safety and in vitro mechanisms of anti-diabetic activity of β-caryophyllene and l-arginine. Journal of Biological Sciences, 18, 124-134. [CrossRef]
42. Bahadori, M.B., Zengin, G., Bahadori, S., Maggi, F. Dinparast, L. (2017). Chemical composition of essential oil, antioxidant, antidiabetic, anti-obesity, and neuroprotective properties of Prangos gaubae. Natural Product Communications, 12(12), 1945-1948. [CrossRef]
43. Younis, I.Y., Khattab, A.R., Selim, N.M., Sobeh, M., Elhawary, S.S. Bishbishy, M.H.E. (2022). Metabolomics-based profiling of 4 avocado varieties using HPLC-MS/MS and GC/MS and evaluation of their antidiabetic activity. Scientific Reports, 12(1), 4966. [CrossRef]
44. Kumawat, V.S., Kaur, G. (2020). Insulinotropic and antidiabetic effects of β-caryophyllene with l-arginine in type 2 diabetic rats. Journal of Food Biochemistry, 44(4), e13156. [CrossRef]
45. Jiang, N., Zhang, Y. (2022). Antidiabetic effects of nerolidol through promoting insulin receptor signaling in high-fat diet and low dose streptozotocin-induced type 2 diabetic rats. Human and Experimental

Toxicology, 41. [CrossRef]
46. Goto, T., Kim, Y.I., Funakoshi, K., Teraminami, A., Uemura, T., Hirai, S., Lee, J.Y., Makishima, M., Nakata, R. Inoue, H. (2011). Farnesol, an isoprenoid, improves metabolic abnormalities in mice via both PPARα-dependent and-independent pathways. American Journal of Physiology-Endocrinology and Metabolism, 301(5), E1022-E1032. [CrossRef]
47. Heendeniya, S.N., Keerthirathna, L.R., Manawadu, C.K., Dissanayake, I.H., Ali, R., Mashhour, A., Alzahrani, H., Godakumbura, P., Boudjelal, M. Peiris, D.C. (2020). Therapeutic efficacy of Nyctanthes arbor-tristis flowers to inhibit proliferation of acute and chronic primary human leukemia cells, with adipocyte differentiation and in silico analysis of interactions between survivin protein and selected secondary metabolites. Biomolecules, 10(2), 165. [CrossRef]
48. Gurumallu, S.C., AlRamadneh, T.N., Sarjan, H.N., Bhaskar, A., Pereira, C.M.F., Javaraiah, R. (2022). Synergistic hypoglycemic and hypolipidemic effects of ω-3 and ω-6 fatty acids from Indian flax and sesame seed oils in streptozotocin-induced diabetic rats. Phytomedicine Plus, 2(3), 100284. [CrossRef]
49. Widyawati, T., Syahputra, R.A., Syarifah, S. Sumantri, I.B. (2023). Analysis of antidiabetic activity of squalene via in silico and in vivo assay. Molecules, 28(9), 3783. [CrossRef]
50. Santos-Sánchez, N.F., Salas-Coronado, R., Villanueva-Cañongo, C., Hernández-Carlos, B. (2019). Antioxidant compounds and their antioxidant mechanism. Antioxidants, 10, 1-29. [CrossRef]
51. Zhang, L., Virgous, C., Si, H. (2019). Synergistic anti-inflammatory effects and mechanisms of combined phytochemicals. The Journal of Nutritional Biochemistry, 69, 19-30. [CrossRef]
52. Uduwana, S., Abeynayake, N. Wickramasinghe, I. (2023). Synergistic, antagonistic, and additive effects on the resultant antioxidant activity in infusions of green tea with bee honey and Citrus limonum extract as additives. Journal of Agriculture and Food Research, 12, 100571. [CrossRef]
53. Mohamed, H., Ons, M., Yosra, E.T., Rayda, S., Neji, G., Moncef, N. (2009). Chemical composition and antioxidant and radical-scavenging activities of Periploca laevigata root bark extracts. Journal of the Science of Food and Agriculture, 89(5), 897-905. [CrossRef]
54. Shafekh, E.S., Khalili, M.A.R., Catherine, C.C.W., Syakiroh, S.Z.A., Habibah, U.A., Norhayati, A.H., Farhanah, N.M.Y., Husna, N.Z., Nafizah, S.M.B., Azlina, M. (2012). Total phenolic content and in vitro antioxidant activity of Vigna sinensis. International Food Research Journal, 19(4), 1393.
55. Zhang, P., Li, T., Wu, X., Nice, E.C., Huang, C., Zhang, Y. (2020). Oxidative stress and diabetes: Antioxidative strategies. Frontiers of Medicine, 14, 583-600. [CrossRef]
56. Gunawardena, H.P., Silva, R., Sivakanesan, R., Ranasinghe, P., Katulanda, P. (2019). Poor glycaemic control is associated with increased lipid peroxidation and glutathione peroxidase activity in type 2 diabetes patients. Oxidative Medicine and Cellular Longevity, 2019, 9471697. [CrossRef]
57. Kastritis, P.L., Bonvin, A.M.J.J. (2013). On the binding affinity of macromolecular interactions: daring to ask why proteins interact. Journal of The Royal Society Interface, 10(79), 20120835. [CrossRef]
58. Battelli, M.G., Bortolotti, M., Polito, L.Bolognesi, A. (2018). The role of xanthine oxidoreductase and uric acid in metabolic syndrome. Biochimica et Biophysica Acta (BBA)-Molecular Basis of Disease, 1864(8), 2557-2565. [CrossRef]
59. Kelley, E.E. (2015). Dispelling dogma and misconceptions regarding the most pharmacologically targetable source of reactive species in inflammatory disease, xanthine oxidoreductase. Archives of Toxicology, 89, 1193-1207. [CrossRef]
60. Hernandez-Hernandez, M.E., Torres-Rasgado, E., Pulido-Perez, P., Nicolás-Toledo, L., Martínez-Gómez, M., Rodríguez-Antolín, J., Pérez-Fuentes, R.Romero, J.R. (2022). Disordered glucose levels are associated with xanthine oxidase activity in overweight type 2 diabetic women. International Journal of Molecular Sciences, 23(19), 11177. [CrossRef]
61. Veith, A., Moorthy, B. (2018). Role of cytochrome P450s in the generation and metabolism of reactive oxygen species. Current Opinion in Toxicology, 7, 44-51. [CrossRef]
62. Gao, H.M., Zhou, H.Hong, J.S. (2012). NADPH oxidases: novel therapeutic targets for neurodegenerative diseases. Trends in Pharmacological Sciences, 33(6), 295-303. [CrossRef]
63. Teimouri, M., Hosseini, H., ArabSadeghabadi, Z., Babaei-Khorzoughi, R., Gorgani-Firuzjaee, Meshkani, S.R. (2022). The role of protein tyrosine phosphatase 1B (PTP1B) in the pathogenesis of type 2 diabetes mellitus and its complications. Journal of Physiology and Biochemistry, 78(2), 307-322. [CrossRef]
64. Frkic, R.L., Richter, K.Bruning, J.B. (2021). The therapeutic potential of inhibiting PPARγ phosphorylation to treat type 2 diabetes. Journal of Biological Chemistry, 297(3). [CrossRef]
65. Vrbanac, J., Slauter, R. (2017). ADME in Drug Discovery. In: A.S. Faqi (Eds.), A Comprehensive Guide to Toxicology in Nonclinical Drug Development, (pp. 39-67). Boston: Academic Press.